



HELSINKI UNIVERSITY OF TECHNOLOGY

Department of Electrical and Communications Engineering

Tero Tuohioja

Methods for industrial manufacturing of LED-integrated optics elements

Thesis submitted in partial fulfilment of the requirements for the degree
of Master of Science in Engineering

Date: 1.11.2006

Supervisor: Professor Pekka Kuivalainen

Instructor: Ph.D. Jarmo Määttänen

Author: Tero Tuohioja	
Name of the Thesis: Methods for industrial manufacturing of LED-integrated optics elements	
Date: 1.11.2006	Number of pages: 81 (8 + 73)
Department: Department of Electrical and Communications Engineering	
Professorship: S-69 Semiconductor technology	
Supervisor: Professor Pekka Kuivalainen	
Instructor: Ph.D. Jarmo Määttänen	
<p>Light-emitting diodes, LEDs, are becoming widely used in illumination applications due to their superior properties, compared to old light sources. However, optics are required with LEDs to ensure improved performance. This thesis concentrates on the integration and replication of optics for LED-based applications.</p> <p>Diffraction optics lenses for light collimation were successfully replicated on LEDs. Both integrated lenses and discrete lenses were fabricated. The production machine was a Toray Engineering Ltd. flip-chip bonder, which is normally used in the electronics industry. Integrated lenses were replicated directly onto the encapsulation material of a LED. The encapsulation material used was a UV curable polymer resin, with a high refractive index. Discrete lenses were also replicated on the UV curable material, but the resin was first dispensed on a 0.25 mm thick PMMA foil. After curing, the foil was cut to a proper size and the lens was attached onto the LED case. The average luminous intensities increased from 291 mcd to 496 mcd and average collimation angles narrowed from 108° to 45°. A slight decrease in luminous flux was observed with the discrete lenses. Integrated lenses did not have any effect on it.</p> <p>Replication of diffraction optics structures was conducted using step hot embossing technology with the Toray bonder. The optical structure type used was a blazed grating. Numerous replications were performed on a 0.5 mm thick PMMA sheet and the success and quality of replication was studied. It was shown that the structures used can be embossed onto a substrate, while maintaining good quality, and that the technology can be industrialized. Step hot embossing replication was also performed on a PMMA sheet with an out-coupling light guide structure on it, and it demonstrated that this technology enables the sheet to be utilized as a signal panel, or as a part of an enhanced illumination backlight system. Over 790% increase in average luminance was measured between the light guide and the embossed structures on it.</p> <p>A highly novel technology called nanoimprint lithography, NIL, was demonstrated using a SÜSS MicroTec NPS300 NanoPatterning Stepper. The NPS300 enables NIL at wafer level on active components, such as LEDs. NIL could be used to improve the external quantum efficiency of a LED without texturing the semiconductor material itself. Oy Modines Ltd. is developing this technology in collaboration with the Technical Research Centre of Finland, VTT.</p> <p>Patents are pending for some of the technologies presented in this thesis.</p>	
Keywords: Replication, diffraction optics, light-emitting diode	

Tekijä: Tero Tuohioja**Työn nimi:** Valodiodeihin integroitavien optisten komponenttien teolliset valmistusmenetelmät**Päivämäärä:** 1.11.2006**Sivumäärä:** 81 (8 + 73)**Osasto:** Sähkö- ja tietoliikennetekniikan osasto**Professori:** S-69 Puolijohdeteknologia**Työn valvoja:** Professori Pekka Kuivalainen**Työn ohjaaja:** TkT Jarmo Määttänen

Valodiodeja (LED) käytetään yhä kasvavassa määrin erinäisissä valaistusaplikaatioissa, johtuen diodien ylivoimaisista ominaisuuksista vanhoihin valonlähteisiin nähden. Diodien rinnalle tarvitaan kuitenkin optiikkaa, jotta niiden hyödyt saataisiin tehokkaasti käyttöön. Tämä työ käsittelee optiikan integrointia ja replikointia diodipohjaisissa sovelluksissa.

Valon kollimointiin tarkoitettuja diffraktiivisia linssejä replikoitiin onnistuneesti valodiodien päälle. Sekä integroituja, että erillisiä linssejä valmistettiin. Replikointilaitte oli Toray Engineering Ltd:n valmistama, elektroniikkateollisuudessa käytetty kääntösirujen liitälaitte. Integroidut linssit replikoitiin suoraan diodin kapselointimateriaalin pintaan. Käytetty kapselointimateriaali oli UV valolla kovetettavaa, korkeataitekertoimista polymeerimateriaalia. Erilliset linssit replikoitiin myös käyttäen UV-materiaalia, mutta materiaali levitettiin aluksi 0,25 mm paksun PMMA kalvon päälle, josta kovetuksen jälkeen kalvo leikattiin sopivan kokoiseksi ja linssi liitettiin diodikotelon päälle. Valovoimat kasvoivat keskimääräisesti 291 mcd:sta 496 mcd:aan ja kollimointikulmat kapenivat vastaavasti 108 asteesta 45 asteeseen. Valovirrassa havaittiin pieni lasku erillisten linssien kohdalla. Vastaavasti integroiduilla linseillä ei näyttänyt olevan vaikutusta valovirtaan.

Diffraktiivisia mikrorakenteita replikoitiin Torayn laitteella askelkuumapainoa käyttäen. Prosessissa käytetty optinen rakenne oli tyypiltään vinohila. Useita kuumapainoja tehtiin 0,5 mm paksulle PMMA kalvolle, josta tutkittiin replikoinnin onnistumista ja laatua. Työssä todettiin, että mikrorakenteiden replikointi hyvällä laadulla on mahdollista ja on täten teollistettavissa. Askelkuumapainoa käyttäen painettiin PMMA kalvosta valmistetun uloskytkävän valojohteen päälle samoja mikrorakenteita ja todettiin, että kalvoa voi täten käyttää signaalipaneelina tai osana parannettua taustavalokalvoa. Mikrorakenteiden keskimääräinen luminanssi mitattiin yli 790% korkeammaksi kuin valojohteen.

Hyvin uusi teknologia, nanoimprintlitografia, demonstroitiin käyttämällä SÜSS MicroTecin NPS300 imprint-laitetta. NPS300 mahdollistaa kiekkoitasolla tapahtuvan, aktiivisten komponenttien kuten valodiodien, litografian. Nanoimprintlitografiaa voitaisiin käyttää parantamaan valodiodien ulkoista hyötysuhdetta ilman, että puolijohdemateriaalin pintaa täytyisi kuvioida. Oy Modines Ltd kehittää tätä teknologiaa yhdessä Valtion Teknillisen Tutkimuskeskuksen, VTT:n kanssa.

Patenttihakemukset jätettiin työn aikana osalle työssä esitetyistä teknologioista.

Avainsanat: Replikointi, diffraktiivinen optiikka, valodiode

Preface

This thesis was written at Oy Modines Ltd. during the summer of 2006. I would like to thank Mr. Leo Hatjasalo, CEO of Oy Modines Ltd. for the opportunity of doing this work.

I would also like to thank M.Sc. Kari Rinko and Ph.D. Jarmo Määttänen, who have given me essential instructions and guidelines for this work. Without them, this work would have not been possible. I also want to thank professor Pekka Kuivalainen, supervisor of this thesis. In addition, I would like to express my gratitude to the boys in the laboratory, Jori Oravasaari and Markku Häkkinen, who have helped me with practical matters, as well as Steve Cantrill-Brown who had time and interest to proofread this entire thesis.

Finally, I wish to thank Annu, for all her support, as well as my family, who have always encouraged me with my studies and my interest in science.

Helsinki, 1.11.2006

Tero Tuohioja

Table of contents

1	Introduction.....	1
2	Fabrication and replication of microstructures	4
2.1	Fabrication of the original.....	4
2.2	Fabrication of the master	6
2.3	Replication methods.....	7
2.3.1	UV- and thermal casting	8
2.3.2	Hot embossing	8
2.3.3	Injection moulding	9
3	Optical microstructures.....	10
3.1	Binary grating	10
3.2	Blazed grating	11
3.3	Curve-type binary grating.....	12
4	Flip–chip bonder	14
4.1	Bonder tools	15
4.1.1	Preparation of two additional tools.....	16
5	Diffraction optics lens replication.....	19
5.1	Materials	21
5.1.1	UV resins	22
5.1.2	Thermal resins.....	22
5.1.3	Material tests.....	23
5.2	Lens replication preparations.....	24
5.3	The replication procedure	27
5.3.1	Integrated lenses.....	27
5.3.2	Discrete lenses	28
5.4	Lens replication tests.....	29
5.4.1	Results.....	29
5.5	Comparison between diffraction and refractive lens	32
6	Step hot embossing	34
6.1	Embossing objectives.....	35
6.2	Success of replication	38
6.2.1	Preparations for analyses	38

6.2.2	Analysing methods.....	40
6.2.3	Test results	42
6.3	Quality of replication	48
6.3.1	Analysing methods.....	48
6.3.2	Results of replication quality	51
6.4	Conclusions for step hot embossing	54
6.5	Optical functionality of step hot embossing	55
7	Wafer level replication.....	59
7.1	Methods for improving LEDs' external quantum efficiency.....	60
7.2	An imprinting approach	62
7.2.1	Demonstration of the process.....	63
8	Applications	65
8.1	Advertisements	65
8.2	Consumers.....	66
8.3	Automotive	66
8.4	Traffic	67
9	Conclusions and outlooks	69
10	References.....	71

List of symbols

f	Focal length
h	Relief height
m	Order of diffraction
M	Number of discrete levels
n	Index of refraction, index
pH	Acidity
p	Grating period
p_{\min}	Minimum zone period
r	Radius of curvature
T_g	Glass transition temperature
Z	Number of zones
δ	Mean square deviation
η_{+1}	Scalar diffraction efficiency of first order
λ	Wavelength

List of abbreviations

3-D	Three-dimensional
CD	Compact disc
CHF ₃	Trifluoromethane
DO	Diffractive optics
DOE	Diffractive optics element
GaAs	Gallium arsenic
HCL	Hydrochloric acid
InGaAlP	Indium gallium aluminium phosphor
LED	Light-emitting diode
MOS	Metal-oxide semiconductor
NIL	Nanoimprint lithography
PDMS	poly(dimethyl siloxane)
PMMA	poly(methyl metacrylate)
RGB	Red green blue
RI	Refractive index
STD	Standard deviation
UV	Ultraviolet
UV-NIL	Ultraviolet nanoimprint lithography
VCSEL	Vertical cavity surface emitting laser

1 Introduction

Light is one of many fundamental things that exist as an integral part of modern living. Light and lighting is required almost everywhere, ranging from general lighting for indoor and outdoor environments, automotive and traffic lighting, to advertisement lighting and consumer products, such as large television panels and mobile communication devices. In all of these areas, the future trend is similar: a vast need for smaller, more durable and efficient products at lower costs and manufacturing times.

Light-emitting diodes, LEDs, are becoming widely used to solve these requirements. The reason for this is in their superior performance compared to existing lighting mechanisms. As LEDs are based on semiconductor technology, their solid-state light producing mechanism is practically unlimited, thus making the component highly durable, also from a mechanical point of view. In addition, energy consumption is far lower with LEDs compared with old lighting methods, such as incandescent or fluorescent lamps. The volumes of LEDs being used are growing every year. Figure 1.1 shows a forecast for LED units consumed around the world.

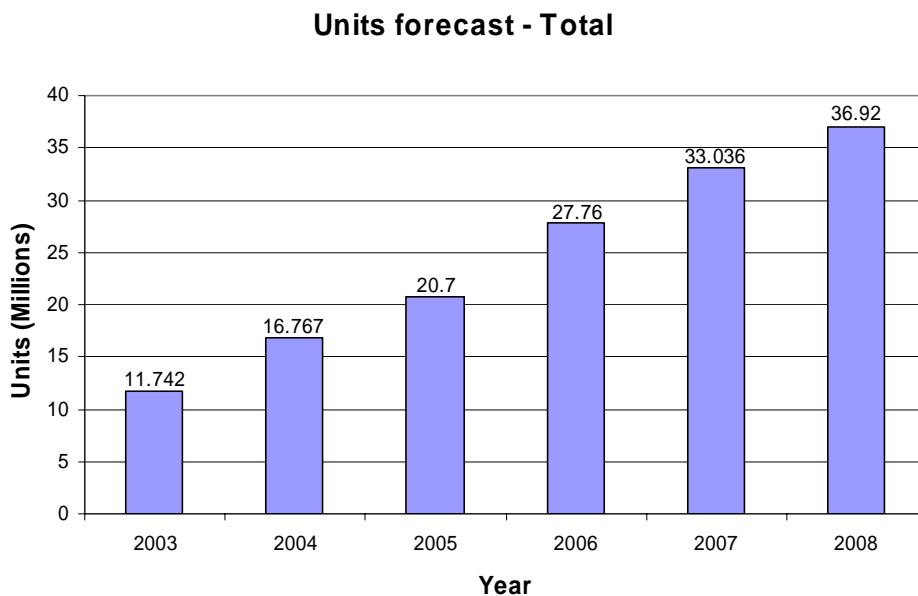


Figure 1.1. Volumes for LED units [1].

Based on this forecast, it is obvious that the LED business is serious and cannot be ignored. For example, the growth between 2006 and 2007 is estimated to be 19%. One reason for the large increase in volumes is explained in figure 1.2. It shows how the price of a LED is going down at the same time as its efficiency is improving.

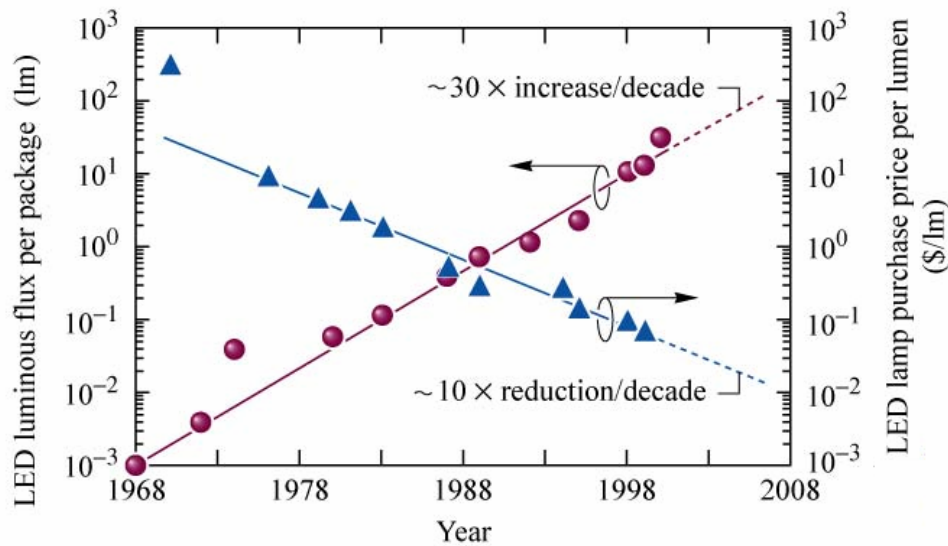


Figure 1.2. Haitz’s law. Diagram showing the price of a LED versus its luminous flux. Every decade the price drops by factor of 10, while its luminous flux increases by a factor of 30 [1, 2].

However, LEDs alone for illumination are not sufficient. Due to their point source nature, there must be also a way to shed the emitted light onto larger areas. To achieve this efficiently, the emitted light should be also properly collimated. All these needs are unattainable for obsolescent technologies that exploit, for example, geometrical optics.

Diffraction optics elements, on the other hand, combined with the LEDs, open up a whole new way of producing light panels or other illumination applications. In addition, this technology goes with future needs. At present, only a fraction of the potential that lays in diffraction optics is utilized. Diffraction optics influences the light at its wavelength level, hence it is capable of doing all the same things as ordinary optics, and even more, but in diminished sizes. Even better, the micro- and nanostructures that are used for this can be copied, replicated, over and over again, which significantly reduces fabrication costs. Additionally, because the materials and

methods that are used for replication are such that the replication cycle times are counted in seconds, it is a wonder that the level of usage of DO is so low.

Even though DO structures are well understood, it is the lack of co-operation between researchers and manufacturers that is delaying the breakthrough in the industrialization of these novel illumination products. Today, LED manufacturers no longer want to be seen as plain LED manufacturers. Instead, they want to be able to offer comprehensive illumination solutions to their customers, and this requires LED-integrated diffractive optics elements. In the past few years, the materials and manufacturing devices have also reached the level where nano- and microstructures are possible to fabricate and replicate, which has created the basis for this work. As replication can be utilized in mass production, LED-integrated DOEs are economical, and the only logical solution for illumination applications in the near future.

This thesis concentrates on the replication of diffractive optics elements and their integration to LEDs and LED based applications. It demonstrates that these novel technologies are also appropriate for industrialization. A manufacturing machine that is used in ordinary electronics industry as a flip-chip bonder has a big role in the success of the demonstrations. Furthermore, it is shown that even at this stage of research and development, the bonder enables fabrications of applications such as DO lens integrated LEDs and enhanced light panels.

First some existing fabrication and replication methods for microstructures are presented, followed by a presentation of microstructures used in this work. After this, the production machine is introduced, and some accessories for it are fabricated. This is followed by an interesting technique in combining a DO lens onto a LED with the help of the bonder. The materials that are used in the process are thoroughly discussed before going on to the optical measurements and results obtained for the lenses. From the presentation and discussion of a technology called step hot embossing, a few experiments are conducted using the bonder, followed by the analysis of the results. After this, a highly novel procedure called nanoimprint lithography is presented and this technique is described and partially demonstrated at wafer level. Finally, before going on to the conclusions and outlooks section, some applications developed by

Modines Ltd. and Modilis Ltd. that could benefit from diffractive optics are introduced.

2 Fabrication and replication of microstructures

Microstructures can be produced many ways, from which the earliest surface relief structures for industrial use, were developed in the sixties when the usage of silicon dioxide in MOS technology was realised [3]. Since then, micro fabrication has developed tremendously, and today when line widths are even on the nanometer scale, the possibilities for creating innovative applications are there for everyone.

When speaking about diffractive optics, the microstructures are in the range of a few hundred nanometers to few micrometers. The use of diffractive optics elements, or DOEs in consumer products have generated more and more interest due to their cost-effective mass production, superior performance, as well as size and weight [4]. The cost-effectiveness is the result of the possibility to replicate diffractive optics microstructures at high volumes, originating from even just one master. Additionally, the fidelity of replicated structures is extremely good in DOEs [5].

2.1 Fabrication of the original

The original is the first object upon which the microstructure is created. Fabrication methods of the original are usually dependant on the structure type of a DOE. The most common type is a binary structure and its fabrication is quite straightforward. Other types are multilevel and continuous profiles, whose fabrications are not trivial tasks, and are therefore disregarded here [6]. A fabrication process of binary profiles is presented in figure 2.1. The basic fabrication steps of binary elements are substrate preparation, patterning, developing, fabrication of the etching mask, and reactive ion etching [7].

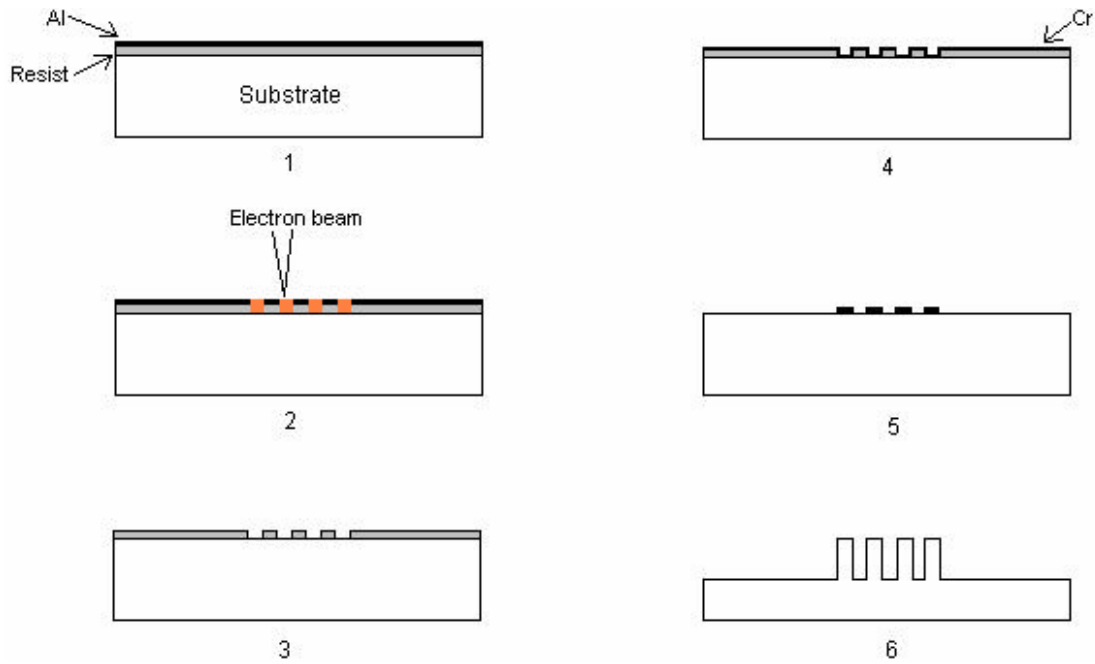


Figure 2.1. Fabrication steps of binary diffractive elements. (1) Substrate preparation, (2) exposure, (3) developing, (4) evaporation of Cr-mask, (5) lift-off, and (6) reactive ion etching [7].

The first fabrication step is the preparation of a substrate for the exposure. The standard resist for electron beam exposure is poly(methyl metacrylate), PMMA. The resist is spin-coated, and after spinning, the resist layer is baked in an oven to evaporate the solvent, and to achieve the final thickness and hardness of the resist. The typical thickness of a resist is in the range of 100 – 700 nm [7].

Because the resist and the substrate are typically both non-conductive, a thin conduction layer is required to avoid the charging effect during e-beam exposure. The conduction layer used, can be, for example aluminium, because it is relatively simple to remove with HCL after exposure. During exposure of PMMA, electrons break the polymer chains on their way through the resist, and the molecular weight is thus decreased in those locations. The developing rate in exposed areas is significantly higher than in non-exposed areas, and the surface profile can, therefore, be obtained [7].

During the developing step, the microstructure is obtained in the resist layer. In principle, the resist microstructure itself can act as a diffractive element, if the resist

thickness is correct. However, the resist structure on the substrate is quite soft, which means poor resistance to mechanical and thermal effects. For better durability, the profile is, in most cases, transferred to the substrate by reactive ion etching. In reactive ion etching of binary profiles the resist is not normally used as a mask, because of the weak relation between the etch rates of the fused silica substrate and the mask. Instead, the structure is transferred into a more resistant material by means of the lift-off technique, where a thin metal layer is evaporated on the substrate. The metal typically utilised here, is chromium. After evaporation, the PMMA layer is removed with acetone, which leaves behind the desired metal mask pattern [7].

Finally, as a result of reactive ion etching, the patterns are transferred into the substrate. Reactive ion etching is an anisotropic etching process, which produces straight sidewalls, thus making it an excellent process for the fabrication of binary structures. The sample is placed in a vacuum chamber and the process gas CHF_3 is introduced and converted to a reactive plasma of charged ions and neutral particles with a power supply [7].

2.2 Fabrication of the master

The master element is created from the original for use in further replication processes. The use of the silica substrate as a master is possible, but not recommended, because silica is highly brittle material and can easily break during a replication process. This is why electroplating with nickel is widely used for making a metal copy from the microstructure in the original. Nickel is the most commonly used material for electroplating because it is significantly harder than, for example, copper or gold. The obtained nickel shim can then be used as a master for further replication of the structure [6, 7].

The original fused silica structure must first be coated with a thin metal film to form a conductive coating for the subsequent electroplating. The metal film has a typical thickness of 10 to 100 nm, and typically, silver, gold, nickel or copper is used [5, 6]. During the electroplating step, the original is set into a nickel sulfamate bath of the

electroforming system. The system, illustrated in figure 2.2, includes two electrodes, a power supply, heater, pump and a filtering unit.

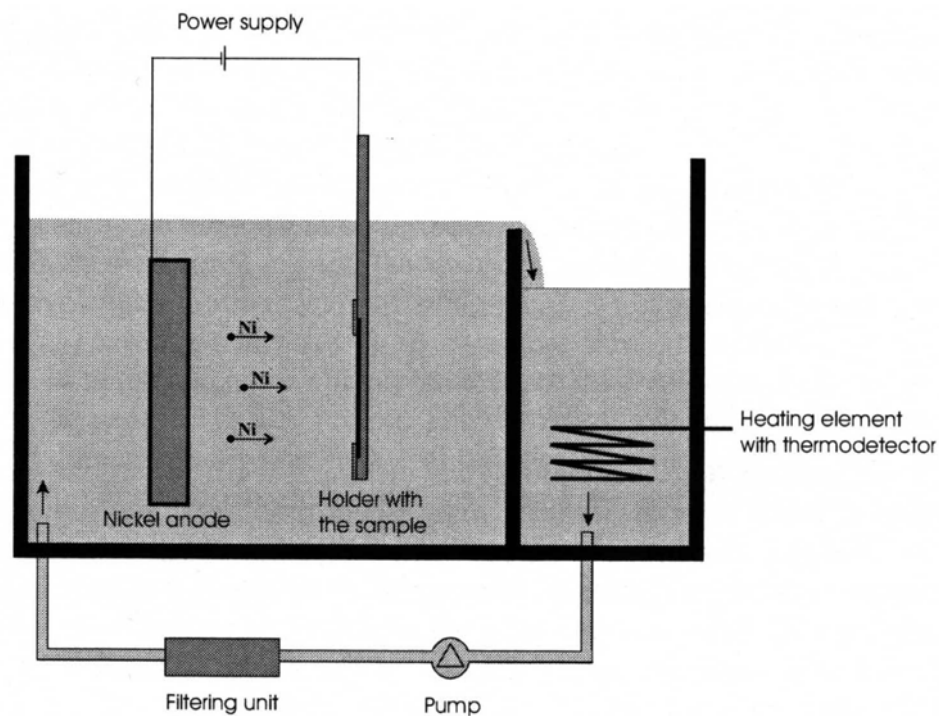


Figure 2.2. A schematic illustration of the system for nickel electroplating [6].

During the process, the original element is connected to the negative electrode, cathode, and set in the sulfamate bath. Positive Ni-ions are attracted towards the negative electrode and the Ni-shim is formed, creating the master element. The thickness of electroplated Ni-shims can vary from 50 μm , to several millimetres depending on the application. To maintain the quality of plated nickel, pH and the chemical composition of the electroforming bath must be continuously controlled. After the process, the master is separated from the original, and any residues are stripped with a suitable solvent [7].

2.3 Replication methods

In the final step of the replication chain, the microstructure of the Ni-shim is transferred into UV- or thermoplastic polymer. The most widely used replication methods include UV or thermal casting, hot embossing and injection moulding, as shown in figure 2.3 [7].

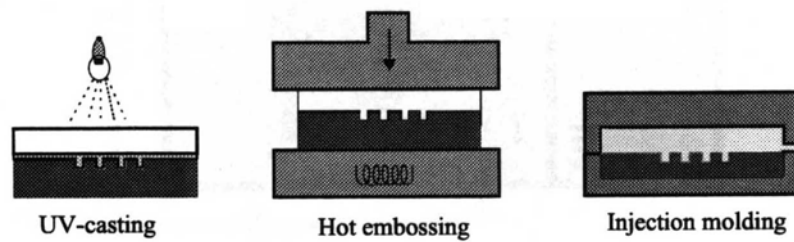


Figure 2.3. Replication methods of diffractive optics structures [7].

2.3.1 UV- and thermal casting

In this method, a UV or thermally curable polymer resin is spread onto a base material, for example, PMMA. The Ni-shim is then placed in contact with the adhesive and immediately cured with an UV-lamp, or in an oven. After curing, the shim and the replica can be separated, and a single replica is produced. UV-casting is more widely used, due to its shorter curing times, ranging from few seconds to couple of minutes. As a result of the short cycle time, UV-casting is an attractive choice for replication [5, 7]. These replication methods will be discussed in more detail in chapter 5.1.

2.3.2 Hot embossing

By using a flatbed hot embossing, the diffractive surface can be replicated into, for example, a thermoplastic polymer. The replication material can either be in the form of a sheet of plastic foil or a thin film, spin-coated onto a substrate. During embossing, the Ni shim is placed in contact with the plastic film, and pressure is applied on the film being heated above its glass transition temperature T_g . After removal of the pressure, the film is cooled down and the Ni shim is removed, leaving a high quality replica of the microstructure. To assist with separation between the Ni shim and the polymer film, a release coating, e.g. a Teflon-like film, may be applied onto the Ni shim before the embossing. Compared to other replication techniques, this kind of hot embossing is relatively slow, with typical cycle times of 10-20 minutes [5].

Roll-to-roll hot embossing, on the other hand, is a mass production method, where cycle times have been successfully decreased along with costs. With this method, the microstructure is on a roller, under which the plastic is fed at high speeds. The plastic is normally above its T_g value and the roller is cooled, thus replicating the structure onto the plastic. However, this fabrication process is still under development and thus, not widely used [8].

2.3.3 Injection moulding

Injection moulding is an established technology for high-speed mass production of plastic components, e.g. compact discs. A Ni shim containing the microstructure to be replicated is mounted on one side of the mould, and preheated plastic is injected into the mould. A pressure of several MPa is then applied. After rapid cooling, the moulded part is extracted, with a cycle time of less than 5 seconds [5].

Nikolajeff *et al.* [5] have been successfully demonstrated in the replication of diffractive optics structures, which were fabricated using a commercially available CD injection moulding machine. The structure depths were around 1 μm and the stability in replication fidelity was maintained over several hundred replicated elements. The replication time was 10 seconds [5]. One of the replicas is shown in figure 2.4.

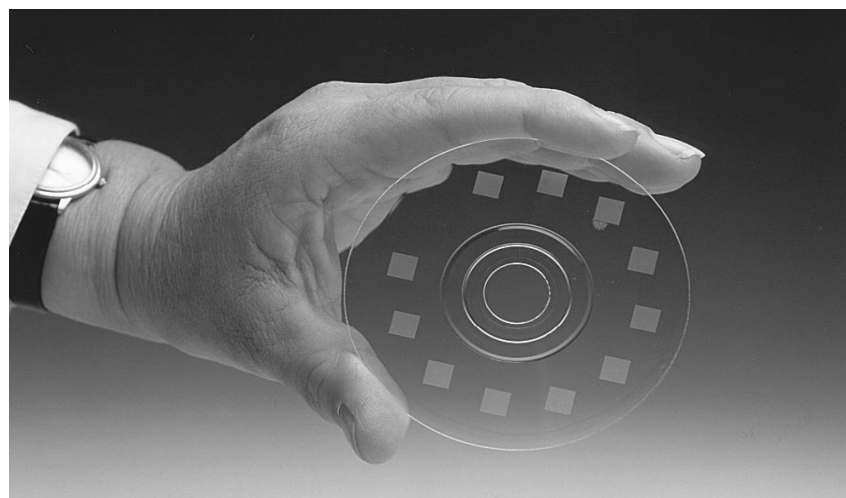


Figure 2.4. A compact disc with several diffractive structures [5].

3 Optical microstructures

Modines and Modilis Ltd. have developed a number of innovative applications, exploiting many different types of diffractive optics structures, from which only a few, important for this thesis, will be presented here. The applications themselves will be described in chapter 8.

3.1 Binary grating

Figure 3.1 shows a single optical unit from a light guide. The entire light guide consists of thousands of these, and similar types of structures. The structures are binary, and thus, the light guide is usually called a binary light guide. The surface of the light guide is modulated so that different kinds of optical units fill the surface at different locations, as illustrated in figure 3.2. The light guides can be designed for all wavelengths of visible light, which means that the application possibilities range from white light backlight panels to emergency signal panels.

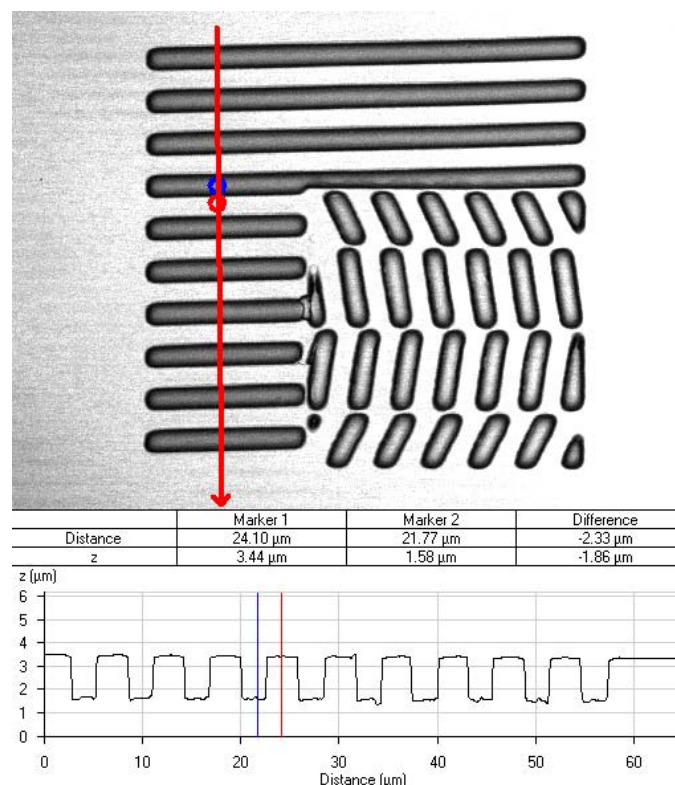


Figure 3.1. An optical unit from a binary light guide.

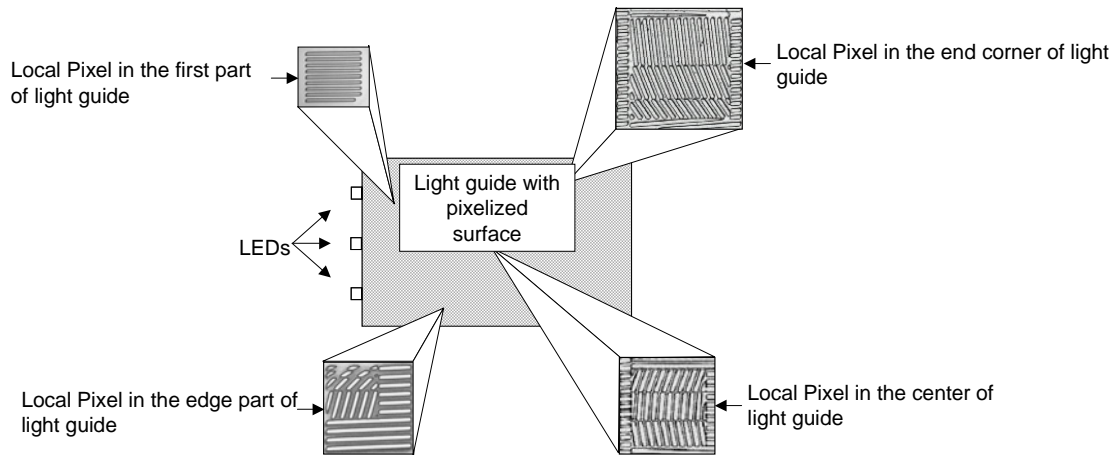


Figure 3.2. Modulated surface enables uniform light out-coupling.

3.2 Blazed grating

Some light guide applications use a blazed grating microstructure for light out-coupling. It is presented in figure 3.3 and is designed to deflect the light progressing horizontally inside a substrate. With Modines applications, the grating is designed to deflect the light at 90° from the incident angle, thus acting like a reflecting mirror. The red line in the picture is produced by measuring software and can be disregarded.

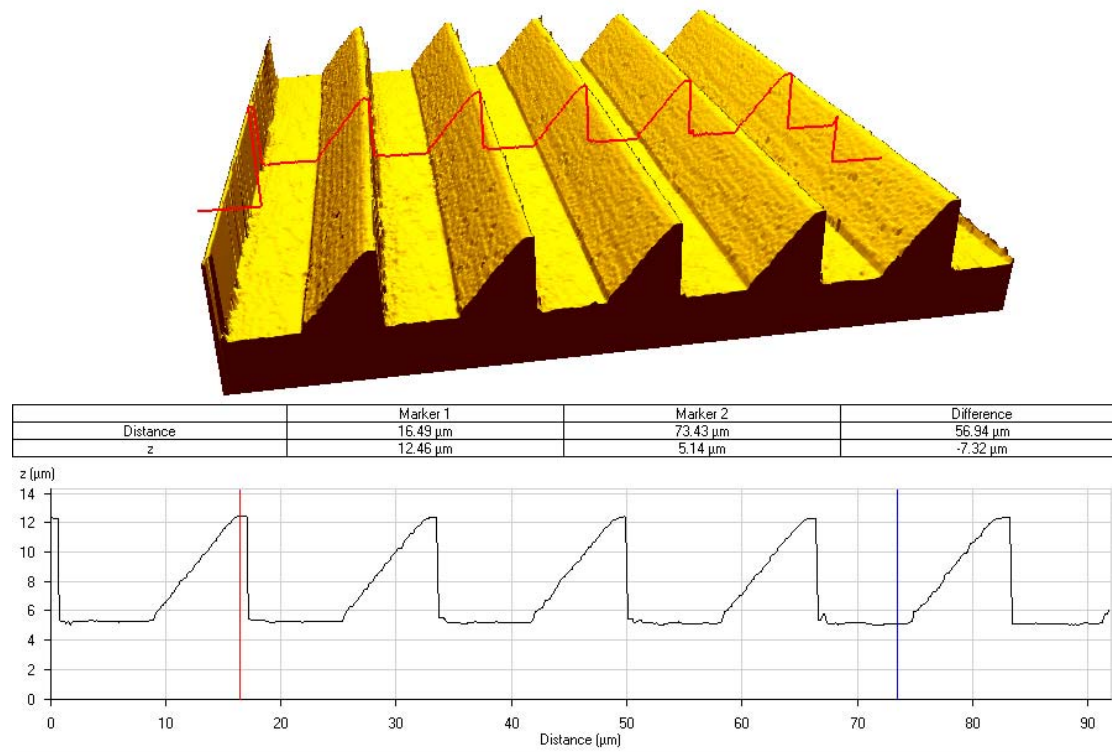


Figure 3.3. Blazed grating structure. The height of the structure is $7 \mu\text{m}$.

The structure in figure 3.3 is of the continuous-type, but there are also binary approximations of the blazed grating. The advantage of using an approximated type is the possibility to use the established lithography methods for fabrication. A four-level binary approximation of the blazed grating structure is depicted in figure 3.4 [5].

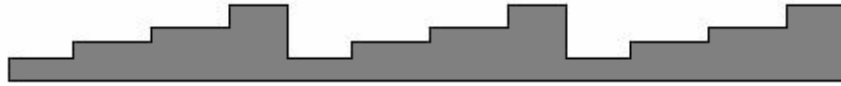


Figure 3.4. Four-level binary approximation of the blazed grating [5].

The price paid for the stepped approximation of the ideal continuous relief is the non-optimal optical performance of the DOE, especially lower diffraction efficiency. The scalar diffraction efficiency in the first order of a blazed grating, as a function of the number of discrete levels M , is given in equation (1) [5].

$$\eta_{+1} = \left[\frac{\sin(\pi / M)}{\pi / M} \right]^2 \quad (1)$$

The 4-level grating shown would ideally give a diffraction efficiency of 81% whereas, in the case of a continuous-relief, the first order diffraction efficiency would be 100% [5].

3.3 Curve-type binary grating

A transmissive DO lens structure for light collimation, used with RGB LEDs, is shown in figure 3.5. An ideal DO lens structure, on the other hand, is shown in figure 3.6. As can be seen, an ideal lens should be based on blazed grating structure, but to be able to fabricate a curved blazed grating, where the zone period becomes shorter when moving radially from the centre, is a very difficult task.

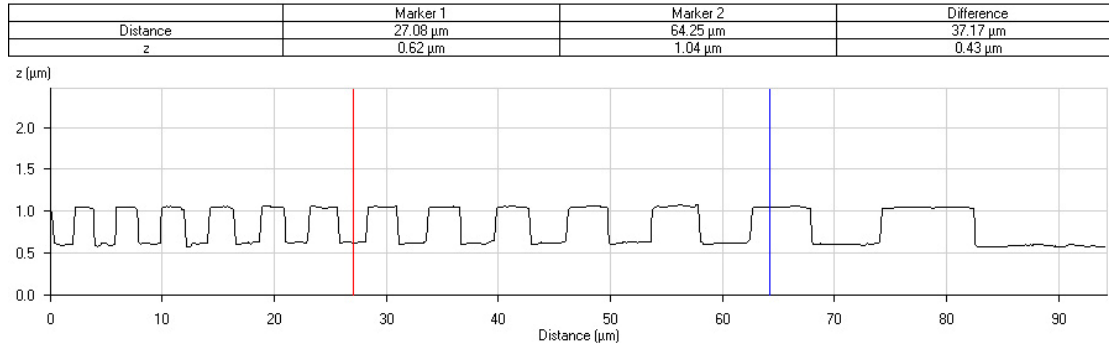
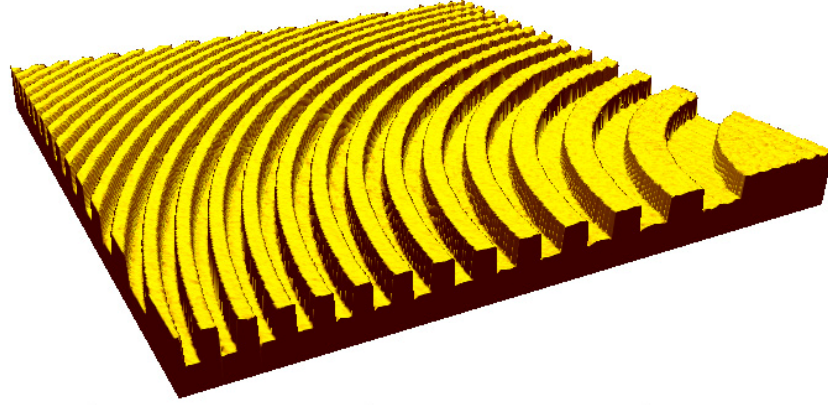


Figure 3.5. A binary structure used in light collimation lenses.



Figure 3.6. An ideal diffractive optics lens structure.

The diffraction efficiency of a DO lens can also be calculated from the equation (1). The Modines lens has a two-phased structure, where diffraction efficiency is 41%, but the fabrication is easier. In fact, the fabrication of an ideal lens structure for the purposes required at Modines would be virtually impossible. For example, the total number of required zones Z for a lens of radius r and a focal length f is given by [5]

$$Z = \frac{1}{\lambda} \left(\sqrt{r^2 + f^2} - f \right), \quad (2)$$

where λ is the wavelength of used light. A Modines collimation lens, with an aperture of 10 mm and a focal length of 2.4 mm, designed for a wavelength of 633 nm, has 4971 zones, calculated using equation (2). Furthermore, the minimum zone period appears at the outermost part of the lens, and for large Z it is given by [5]

$$p_{\min} = \frac{\lambda(f + Z\lambda)}{r}, \quad (3)$$

which gives with the values above for the minimum zone period of 702 nm for the Modines lens. The height of the structure depends on the wavelength used, and is typically sub-micron – 430 nm in the figure 3.5, for example. All the above requirements for the structure constrain to use binary profiles. In addition, replication with good quality would be impossible for ideal structures.

4 Flip–chip bonder

This chapter introduces the machine that will be used in this thesis for the demonstration of automated replication processes. The Toray Engineering Inc. flip-chip bonder is a mass production machine for the electronics industry, which bonds small chips onto circuit boards using heat curable anisotropic paste. The paste contains metal particles of few microns in diameter that make the paste conduct when two contact areas are bonded together. The entire bonder is shown in figure 4.1A and in figure 4.1B the worktable and the bonder head are shown. These are key components in the machine.

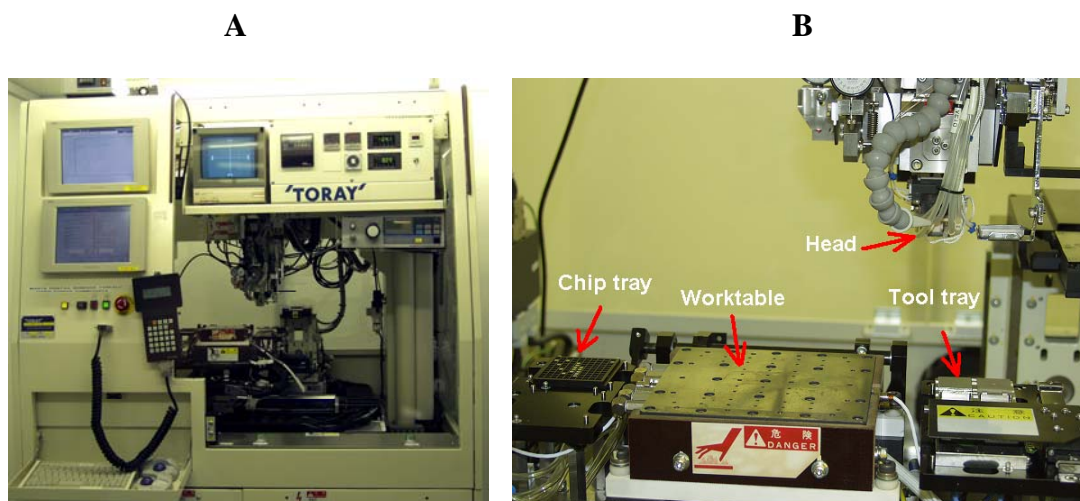


Figure 4.1. The complete bonder in figure A, and the key components in figure B.

It is possible to attach different kinds of tools for different sizes of chips onto the head. Attaching a tool is done by vacuum, from a tool tray. In normal use, a circuit

board is placed on the table where there are vacuum holes to keep the board in place. The head picks a chip from a specific tray onto its tool tip, by vacuum, and then bonds the chip onto the board using heat and pressure. Prior to this, it has of course, dispensed a small drop of the paste onto the circuit board. In automatic mode, the machine picks a chip and rapidly moves to the next position. The primary limiter to the whole bonding cycle is the time it takes to cure the paste.

The table moves in x and y directions, and the head moves in z direction. There is also a $\pm 10^\circ$ swing angle for the table. The machine is highly accurate, as the x and y movement precision is $0.5 \mu\text{m}$ and the z movement precision is $5 \mu\text{m}$. These precisions also hold across the entire movement ranges, which are several centimetres in every direction. The head temperature is controllable to as much as 400°C and the heating is instantaneous, due to the use of an induction heater. It is also possible to adjust the pitch of the head in x and y directions to assure perpendicularity. Regarding pressure, there are two ranges, low pressure and high pressure. Low pressure is up to 16 N force, while high pressure is from 16 N to 150 N force. Switching from one range to another must be done manually, and cannot be done on the fly. The pressing force is set in the bonder as kilograms (Newtons) and is indicated simply as pressure. Even though pressure is bounded to an area and its SI unit is Pascal, it is more illustrative here to speak about pressure and use Newtons as units rather than speak about force. Thus, it has been decided that, in context with the bonder, this arrangement will be used from now on.

4.1 Bonder tools

One of the original, factory-made bonding tools is shown in figure 4.2A, while its dimensions are shown in figure 4.2B.

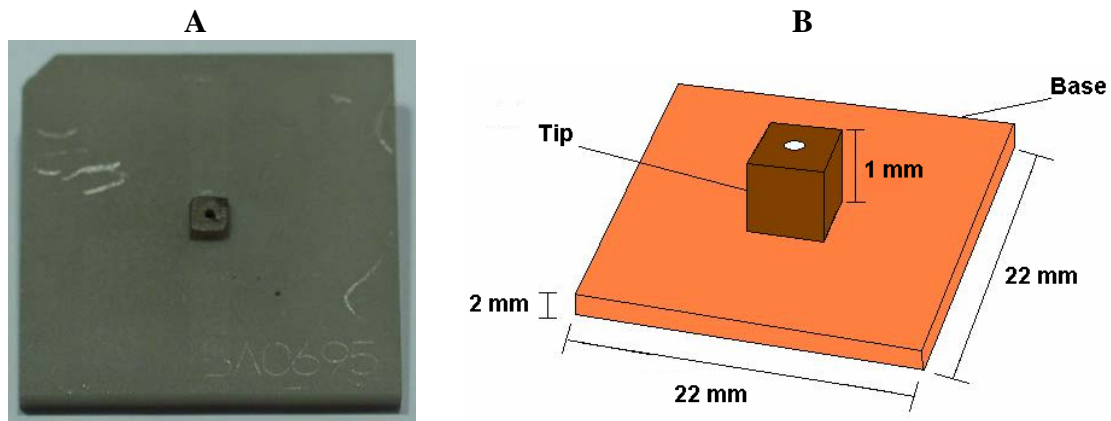


Figure 4.2. Original bonding tool in **A** and its schematic presentation in **B**.

The tip, and the base thickness dimensions may alter, but the overall thickness of the tool must be 3 mm. The official tools are ceramic, and are made so that the coefficient of heat expansion is almost nonexistent, and the flatness of the base is sub micron. This is because, when working with induction-heated tools the dimension variability has to be kept to a minimum. Flatness is also very important, even more so than dimension stability, because if even a small particle gets between the tool and the head, or the tool base is not smooth enough, the bonder does not obtain a vacuum as required. The drawbacks of these ceramic tools are, that they break easily if dropped, and are expensive.

4.1.1 Preparation of two additional tools

For this work, two hand made tools were prepared for use in technology to be described later in this paper. The mandatory dimensions were also fulfilled, without any high precision tools. The base in both tools is of 2 mm thick aluminium, which was sawn and filed to size. In an original tool, there is a small hole in the centre of the tool for chip vacuum. For these metallic tools, no chip vacuum holes were needed, which led to a small amount of customisation of the bonder. At the end of each bonding cycle, the machine performs a chip blow to ensure that the chip detaches from the tool. As there are no holes in the metallic tools, the chip blow would have shifted the tool itself on the head. This is why the chip vacuum hose was removed.

Next, tips for the tools were fabricated. The tips were made from the optical blazed grating structure, introduced earlier. From an A4 sized nickel shim, with a surface completely filled with the structure, a smaller piece was sawn off. The piece of shim, 1 mm thick, is combined with the base, thus equalling the required 3 mm. It was designed that the tip should be round, 1 mm in diameter. To accomplish this without damaging the structure, a stamping method was used. The stamp was a drill socket with a 1 mm hole, which is shown in figure 4.3. Nickel is a rather hard metal, so to be able to press it down, the stamp had to be made from chilled steel.



Figure 4.3. The stamp, made out of a drill socket, is in a custom-made sleeve.

For stamping a compressing device was used, onto which the stamp was attached. This is shown in figure 4.4. The piece of nickel was placed under the stamp and pressed slowly under a force of 10 kN, which is the device's maximum. The outcome was a round tip as specified. Finally, the piece was glued onto the aluminium base with epoxy, as it tolerates high temperatures.

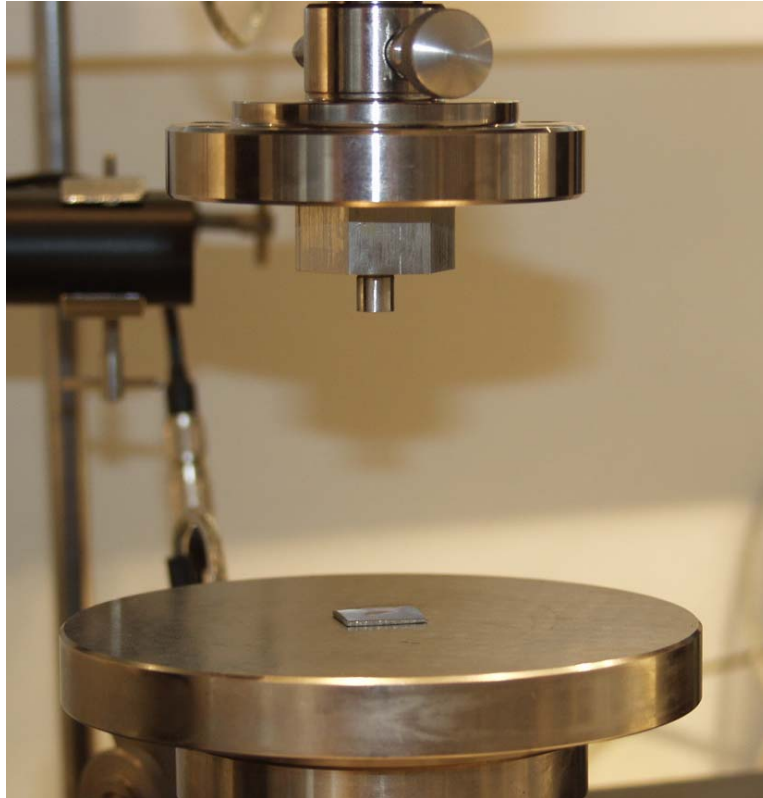


Figure 4.4. A piece of nickel being stamped in a compressing device.

The first tool tip that was prepared is shown in figure 4.5. The tool itself will be known as tool A from this point on.

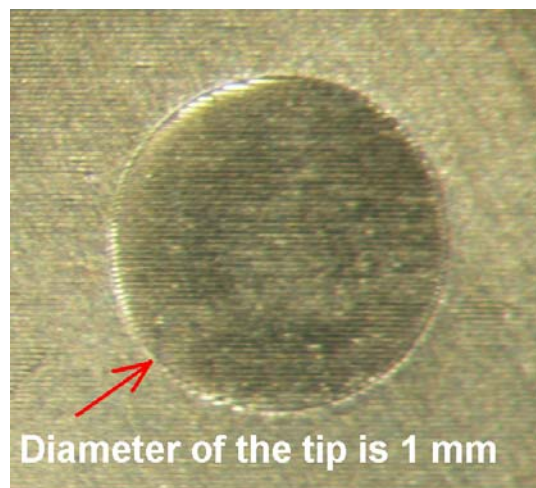


Figure 4.5. A stereomicroscope image of tool tip in tool A. With careful observation, one can see the horizontal grating lines. There are a total of 63 grating lines in the tip.

The speciality of this tool is that the tip is only as high as the optical structure, meaning a height of just a few micrometers. Consequently, the area around the tip

should be at the same level as the bottom of the structure of the tip. The meaning of this will be discussed later.

The second tool tip is shown in figure 4.6 and the tool will be called as tool B. This tool has a noticeable tip, as it is several hundreds of micrometers higher than the rest of the nickel. The meaning of this will be discussed later in this paper.

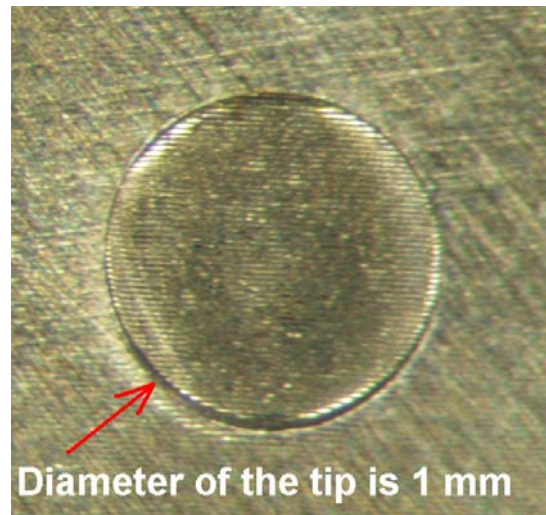


Figure 4.6. A stereomicroscope image of tool tip in tool B.

Both of the tools were quite successful from a microstructure point of view, and the bottom plates of the tools were smooth enough for the bonder head to attach to them by vacuum. The head's pitch in the bonder had to be adjusted, though, for both the tools.

The prepared tools can now be used in a replication process where the blazed grating structure will be transferred to a substrate. This procedure will be discussed in chapter 6.

5 Diffractive optics lens replication

Light collimation is one of the main objectives at Modines Ltd. When light is better collimated, the dispersed light is reduced, which makes it possible to couple the light

more efficiently. Numerous applications could take advantage of high-collimated light.

Collimation is achieved with diffractive optics lenses, which can be small in size but which gather and collimate the light from the whole luminous surface, like the surface of a LED. The advantage of using a DO lens over a traditional lens is the possibility to attach the lens straight onto the LED making the whole assembly very compact. In addition, DO lenses are suitable for replication, hence making costs for one lens low. Lenses to use for collimation are well known and understood, but combining them to LEDs is still at prototype level – there is no efficient and economical way, as yet, to produce LEDs with DO lenses. In this chapter, two innovative solutions to combine a lens to a LED will be introduced, and it will be shown that these methods are also appropriate for industrial manufacturing.

A lens can be attached to a LED in two ways. Either the lens is discrete, or the lens is replicated straight onto the encapsulation material of the LED. In the first approach, the lens is replicated on a polymer resin, which can be of either a UV, or a thermally curable type. The resin is first thinly dispensed onto a polymer film, for example, PMMA, and the lens master is placed in contact with the resin. Next, the resin is cured, either with an UV lamp or in an oven, yielding one replicated lens. The polymer film is cut to size and the lens is attached to an appropriate LED case.

The second approach uses the curable material, directly, without any films between. There are LEDs on the market, which can be bought without encapsulation. The LED die is in a small LED case, which can be filled with the resin, and when placing the master on the resin and curing it, the lens is formed on the encapsulation. The LEDs used in this thesis were amber Osram power TOPLEDs without encapsulation – as shown in figure 5.1. These LEDs are lambertian emitters, giving a 120° opening angle for the light, and they are based on InGaAlP technology [9].



Figure 5.1. An Osram power TOPLED used in this work [9].

5.1 Materials

As mentioned earlier in this paper, there are both UV and thermally curable materials on the market, which are appropriate for diffractive optics lens replication. There are few requirements regarding the materials though, which are important to understand when performing replication. In order to replicate microstructures efficiently, the material has to have quite low surface tensions, low flow properties, and the mould shrinkage value should also be low. These issues ensure that all small cavities etc. will be filled and that after curing, the formed structure will keep the same form, and remain unchanged. The cured material should tolerate high temperatures, because if lens replication is performed during the early process steps of LED manufacturing, it is at the reflow step at the latest, where this requirement shows its value. Other requirements include resistance to abrasion and hydrolysis. Chemical resistance to various solvents is also desirable. In addition, adhesion to other materials is necessary. Most of the materials on the market fulfil these requirements. It is the optical properties that make the differences between them.

The materials must be optically transparent. This means that visible light transmission must be over 90%. Furthermore, they must not show any yellowing during curing. Although a material might not absorb light, it can turn yellow, which is not acceptable in transmissive optics where white light, for example, is used. This is where the first distinguishing factors between materials become apparent. The most important optical property is the refractive index of a material. LEDs are usually based on InGaAs or similar technologies, where the refractive indices are typically around 2 – 3.5. When a LED produces light straight into air, for example, and where RI is 1, a significant amount of total internal reflection of light will occur in the LED die, due to the high difference between the RI values. This will cause only a fraction of the light to be

emitted out. If the die is encapsulated with an optical material, with an RI of 1.5 or higher, more light will naturally be emitted out. Theoretically, all the light that is not recombined in the die would escape if an optical material had the same RI value as the LED die.

5.1.1 UV resins

Optical UV materials are one-component polymer resins that require ultraviolet light to start the cross-linking of the polymer chains, and they are typically based on acrylic technology. The UV dose required is usually $1 - 5 \frac{J}{cm^2}$, which is achieved for instance, with a lamp that produces over $100 \frac{mW}{cm^2}$ of UV light, which is easily obtained because a typical UV lamp normally produces over $40 \frac{W}{cm^2}$. The wavelength of the light should be in the range of 250 – 400 nm. The time it takes to cure the material varies from few seconds to couple of minutes, depending on the thickness of the resin layer, the UV lamp used, and the distance of the light source. UV curable resins are popular, due to their ease of use and fast curing properties. Some UV materials on the market fulfil all the requirements for an optical adhesive.

5.1.2 Thermal resins

Thermally curable materials are usually based on epoxies. Both one- and two-component epoxies are appropriate for replication. The temperature range typically required for curing is from 80 °C to 200 °C. The advantages of epoxy-based resins over acrylic materials are higher RI values, which can be over 1.7, better heat resistance and superior adhesion to materials. Disadvantages are long curing times, varying from few minutes to hours, depending on the temperature, and the mixing of the two components to a specific ratio.

5.1.3 Material tests

For this work, five adhesives were tested for lens replication, and these are presented in table 5.1. Both UV and thermally curable materials were selected for the test. The parameters in the table are from the materials' datasheets.

Table 5.1. Materials that were tested.

Manufacturer / Material	Curing	RI / 580 - 633 nm	Thermal stability / °C	Transparency / %	Viscosity / Pa-s	Technology	Remarks
Micro Resist Technology / ORMOCOMP	UV / Thermal	1.52	> 250	>90	2 - 6	Acryl	Yellowing during UV curing
Luvantix Co. Ltd / EFIRON OA 2062 HNG-T	Thermal	1.668	> 200	>90	0.35	Epoxy, 2 comp.	The formed texture is granular
Addison Clear Wave / AC L2007-K2	UV	1.57	> 200	N/A	2.5 - 3.5	Acryl	45 °C may start the polymerization
Electronic Materials Inc. / OPTOCAST 3590	UV	1.545	> 200	N/A	3.5	Epoxy, 1 comp.	Yellowing at high temperatures
Norland products Inc. / Optical adhesive 65	UV	1.52	> 250	> 95	1.2	N/A	65 °C may start the polymerization

Basically, optical functionality and heat resistance were the two main issues investigated. Optically it is important that the material shows no yellowing, and this was tested under heavy UV dosing. The degree of yellowness after the exposure was an ocular estimate. Thermal resistance was tested in an oven under increasing temperatures. A microstructure was also replicated onto the material, before heating, to indicate possible structure defects etc. after heating. These were investigated using a microscope. The heating procedure is shown in figure 5.2. This imitates a typical infrared reflow soldering profile used in LED manufacturing [9]. The time and temperature values, though, are application dependant.

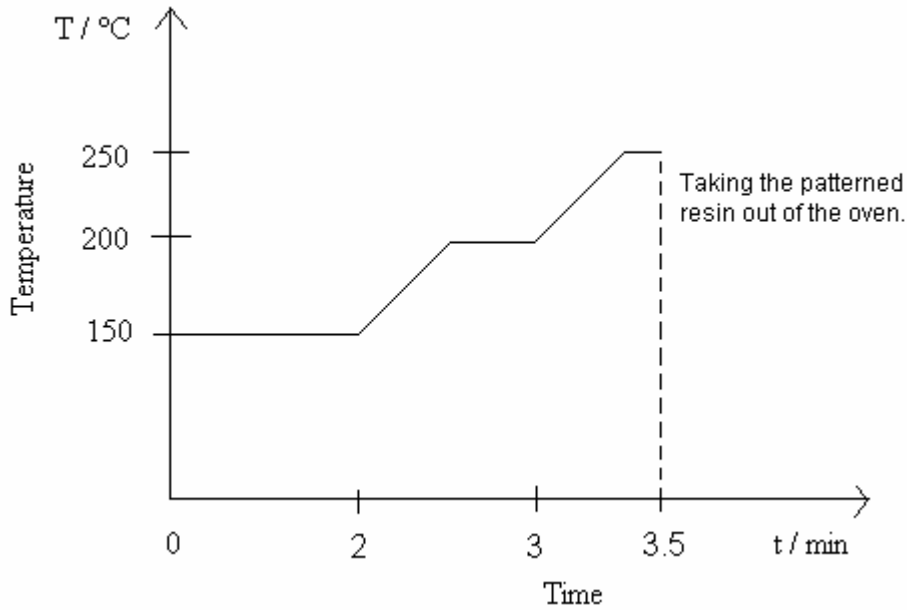


Figure 5.2. Thermal resistance test diagram.

Materials by Addison Clear Wave and by Norland were the two resins found to be the best, as they showed no yellowing, and the replicated structures seemed to be intact after heating. The lens replication tests, however, were performed using the ACW material, due to its higher RI value.

5.2 Lens replication preparations

Both of the lens types were fabricated; discrete lenses and integrated lenses. The manufacturing machine used in the process was the Toray bonder. The bonder was not equipped with an UV lamp, which means that some customisation of the machine was necessary. As explained earlier in chapter 4.1.1, the chip vacuum hose was taken off to disable the chip blow. Using a thin optical fibre, like those used in surgical situations, it was possible to penetrate the fibre into the chip vacuum hole from the side of the head. This is shown in figure 5.3. This allows the UV resin to be cured from above.

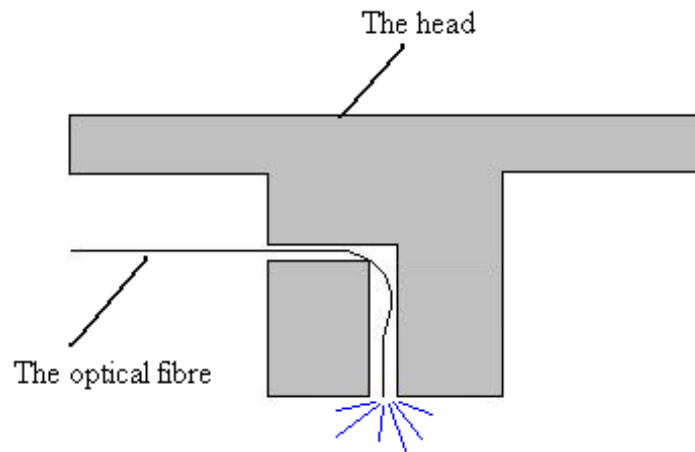


Figure 5.3. Schematic presentation describing the procedure for placing the optical fibre into the chip vacuum hole.

The lens structure is patterned onto a fused silica plate. It is not possible to use the glass original directly, but making a PDMS, also known as silicone, replica from it enables the structure to be replicated further. It was invented to utilize one of the original bonding tools for the process. Figure 5.4 shows the tool used, from which the chip vacuum hole in the middle can be seen.



Figure 5.4. The original bonding tool.

The hole is about the same size than the optical structure, so by placing the tool upside down on the lens structure on the glass and filling the hole with silicone, the structure will be replicated on the tip of the tool. This procedure is shown in figure 5.5A and the final product in 5.5B.

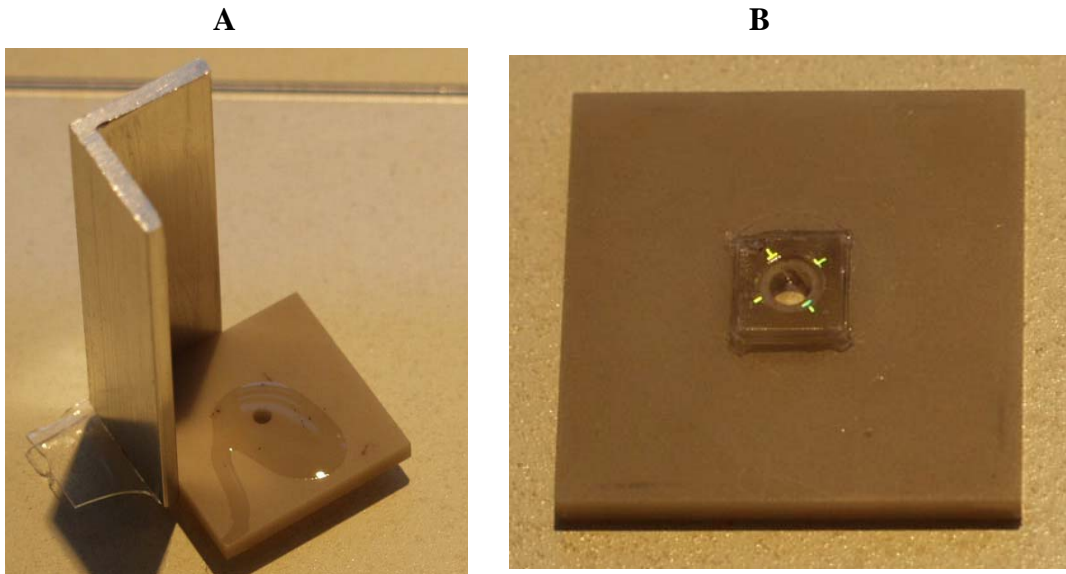


Figure 5.5. The chip vacuum hole filled with silicone in **A** and after curing the silicone lens master is formed on the tip of the tool in figure **B**.

Because silicone allows UV light through without much absorption, the tool works perfectly in automated replication of diffractive optics lenses. The functionality of this procedure is illustrated in figure 5.6.

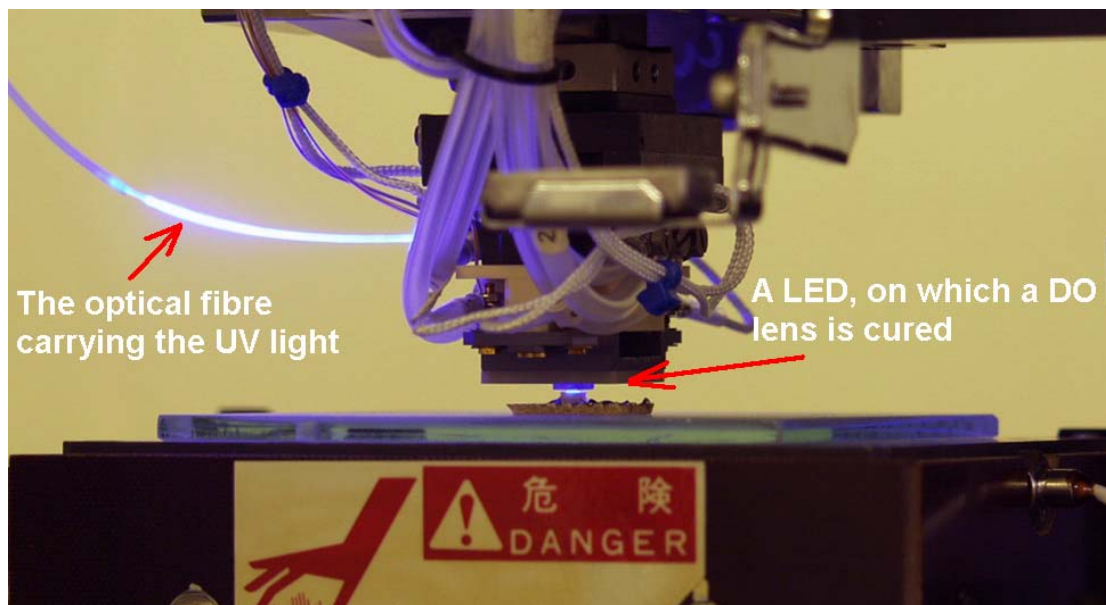


Figure 5.6. An integrated diffractive optics lens being cured on a LED through an original bonding tool.

During preliminary tests, it was discovered that the resin cured slowly, and only from a small area. The reason for this was believed to be the fibre. Basic optical fibres are

designed to carry visible light efficiently, which means that much of the UV light was absorbed by the fibre. In addition, because the aperture of the fibre was small, the light was focused on a small area. Additionally, only a portion of the UV light power was coupled into the fibre. This drawback forced to find out another approach. However, with the right kind of a fibre, the idea should be fully functional.

Because the curing could not be performed efficiently enough from above, a pure PDMS tool that has the lens structure replicated in the middle, replaced the ceramic tool. Curing was performed using a UV lamp directly. The lamp was put close proximity to the bonder head, and to ensure curing, the light was left on for several minutes during each lens replication. To boost the curing of the resin, the top of the silicone tool was covered with a reflecting tape to direct the UV light down, onto the resin.

5.3 The replication procedure

5.3.1 Integrated lenses

The procedure was quite straightforward in both replica types. The integrated lenses were fabricated by attaching first the silicone tool onto the bonder head. The LED was then attached to a plastic board and placed on the worktable. The bonder has a dispenser unit, which produces small paste drops during the process of flip-chip bonding. This unit can be used in the lens replication process. The only changes that need to be made are for the paste syringe to be changed and replaced by a UV resin syringe and some adjustments made to the amount of dispensing. In this work, however, the dispenser was not used and the dosing of the resin was done manually. Using a syringe and a thin needle, the resin was injected into the LED case. The amount was an ocular estimate, but the rule of thumb was that when a small dome formed on the LED case, the amount of the resin was deemed as sufficient. Usually 3-5 drops of the resin were enough.

The alignment of the lens onto the LED was the most delicate phase in this process. The bonder is equipped with a double camera, which can be moved in x, y and z directions. The two cameras are placed in vertical positions, opposite to each other, so

one looks up and the other down. The double camera combination can be placed between the head and the worktable. First, by looking with the upper camera and aligning its cross wires in the centre of the lens structure on the tool, the camera is aligned. By switching to the lower camera and by moving the worktable aligning the LED die in the centre of the lower camera's cross wires, the lens structure on the tool is aligned to the LED. The camera is then pulled back and the head is lowered until the tool is in contact with the LED case. Finally, the UV lamp is placed nearby and switched on. The final step is presented in figure 5.7.

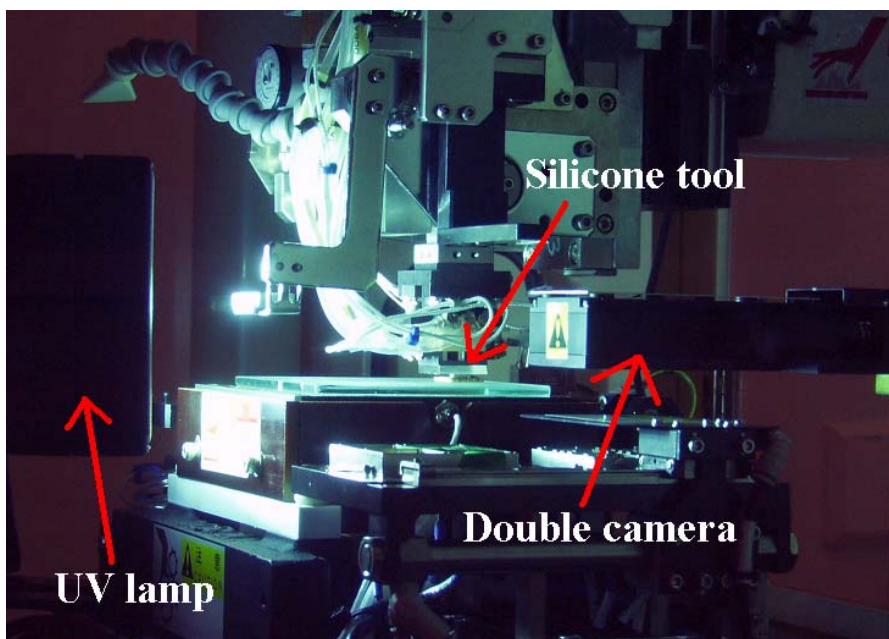


Figure 5.7. A lens being cured using a UV lamp. The lamp is on the left side of the picture and the double camera on the right.

5.3.2 Discrete lenses

The fabrication of discrete lenses was even simpler. A 0.25 mm thick PMMA sheet was placed on the worktable and a small drop of the resin was dispensed onto it. The head was lowered until the resin was compressed between the tool and the sheet. Alignment is not so important in this procedure because the resin will spread over the whole tool area during compressing. The UV lamp was again placed close by and switched on. After curing, the formed lens was cut off. The alignment of the discrete lens onto the LED was challenging. It was done under a stereomicroscope using pair of tweezers and instant glue.

Although the end of this process required a lot of manual work, it is most definitely applicable in an automated process, with the Toray bonder, for example. The only requirement is an appropriate cutting tool for extracting the lens from the substrate, and because the bonder is designed for pick-and-place situations, the application is ready.

5.4 Lens replication tests

Three integrated lenses and three discrete lenses were fabricated and analysed. The integrated lenses were replicated onto three different LEDs, whereas the discrete lenses were attached on the same LED one at a time. The LED used with the discrete lenses was also a reference LED. The reference was fabricated by filling the LED case with the resin, with no structures were patterned on it. All the LEDs were from the same fabrication batch, so the assumption was that they were uniform in quality. In total, eleven LEDs were available for the tests.

The measurements included both spectral and angular luminous intensity measurements, as well as luminous flux measurements. These were done for all integrated lens LEDs, and after each attached discrete lens. Additionally, the reference LED was measured before and after encapsulation. Furthermore, three other LEDs that were not included in the actual tests were also measured before encapsulation, just to be sure of the batch's uniformity. The forward current was 20 mA in all measurements. The light collimation angle was obtained from the angular intensity measurements. The established custom is to give the angle value, measured from the half intensity point.

5.4.1 Results

To give an illustrative picture of the functionality of the collimation lenses, figures 5.8 – 5.10 show first the angular intensities of the reference LED, integrated lens no. 2 and discrete lens no. 2, respectively. The figures show how the emitted light is collimated through the lenses. A stereomicroscope image of the LED and lens used is also presented. The width remains same with all LEDs.

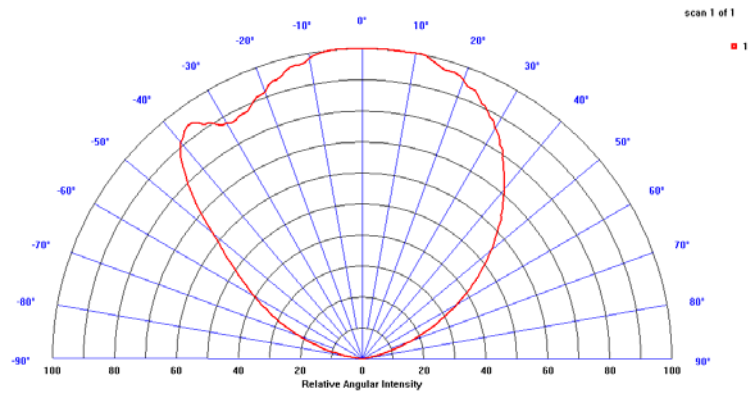
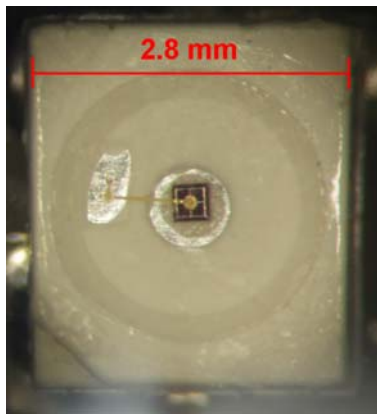


Figure 5.8. Angular intensity of the reference LED.

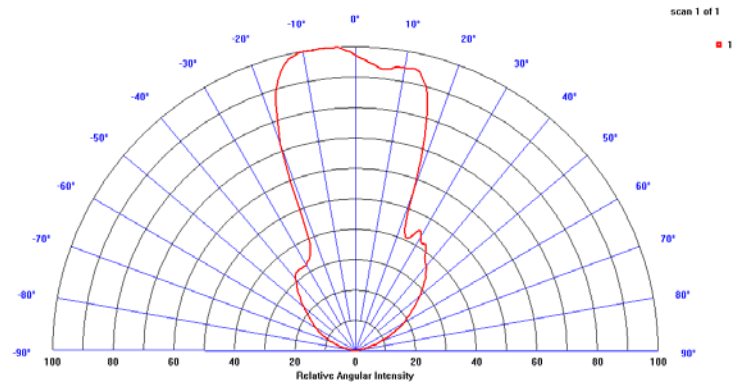
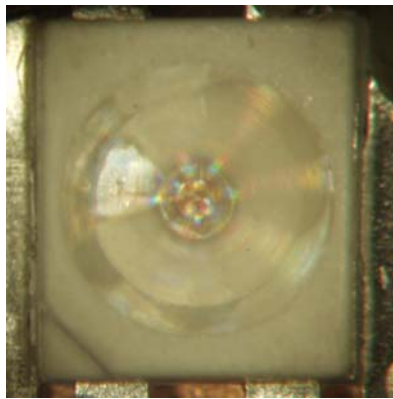


Figure 5.9. Angular intensity of integrated lens number 2.

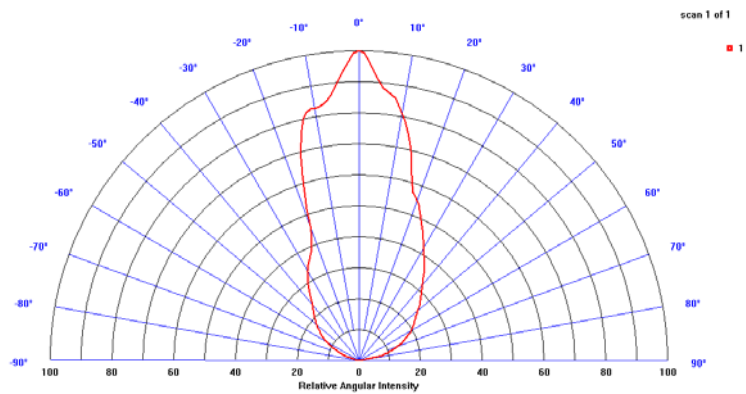
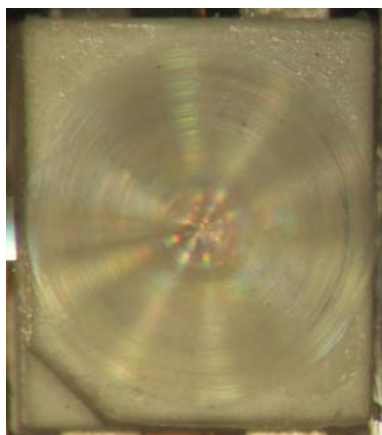


Figure 5.10. Angular intensity of discrete lens number 2.

In table 5.2 the measurement values from reference LEDs without encapsulation are presented. The results from the optical measurements for the LEDs with lenses, on the other hand, are presented in table 5.3.

Table 5.2. Some LEDs before encapsulation. Ref is the same LED in table 5.3.

	LED No.	Luminous flux / mlm	Luminous intensity / mcd	Collimation angle / °
LEDs without encapsulation	1	450	200	113
	2	470	200	102
	3	460	185	112
	ref	460	195	111

Table 5.3. Test results for the LEDs with lenses.

	LENS No.	Luminous flux / mlm	Luminous intensity / mcd	Collimation angle / °
Integrated lens	1	800	468	49
	2	686	515	43
	3	633	464	47
Discrete lens	1	590	494	37
	2	574	660	45
	3	602	377	47
Reference, encapsulated LED without lens	ref	631	291	108

The first thing one observes is the severe increase in luminous flux after encapsulation. It seems that these LEDs provide around 450 mlm before encapsulation and over 600 mlm after encapsulation. The increase is obvious, and due to the refractive index issues explained in chapter 5.1. LED number 1 in table 5.3 is an exception, as it has notably higher luminous flux than the others. The reason for this is in the LEDs themselves, as the LED manufacturer gives quite a large luminous flux scale for the LEDs, even inside the same fabrication batch.

The second thing that is clearly seen is that discrete lenses decrease the luminous flux whereas integrated lenses do not seem to have any effect to it. This is simply because with the discrete lenses there are two separate materials affecting the outcome, as well as the air between them. The PMMA film absorbs some of the light, thus decreasing the luminous flux. The highest luminous intensity, however, is obtained with a discrete lens number 2. This is because this lens type is designed for use as a discrete lens, but it was used as an integrated lens too, to demonstrate the technology. Despite

this, the second integrated lens gives quite a good intensity value as well. As a result of the fabrication procedure in attaching a discrete lens on the LED was a manual operation, it is obvious that the variation between the intensity values in discrete lenses is large. Integrated lenses are better in this respect. The collimation angle value for this lens type is designed to be around 40° , which is clearly achieved.

The results speak for them selves. In all cases, the intensity values increased and the collimation angles became narrower, down to desirable values. The use of the Toray bonder showed that this kind of lens replication also works in automated processes, hence enabling mass production of LEDs with diffractive optics lenses. Of course, there are lot of problems to be solved before there are LEDs on the market with DO lenses. At this stage of integrated lens fabrication, the lens structure is unprotected, and as such, is vulnerable to scratches. One solution for this could be another encapsulation layer, but more material will mean more losses in luminous flux, and possibly, a drop in intensity as well. On the other hand, due to the nature of the binary structure, the discrete lenses can be placed upside down on the LEDs, enabling a cover for the lens structure, but the attaching procedure must be done carefully. Despite the problems that still exist, the fabrication methods are proven here as showing potential.

5.5 Comparison between diffractive and refractive lens

The LED manufacturer also provides LEDs with integrated lenses. The lenses used are based on geometrical optics and one is shown in figure 5.11.



Figure 5.11. An Osram power TOPLED with the manufacturer's collimation lens [10].

The lens is quite big compared to Modines lenses, which are on the same level as the LED case. To give yet another reference, this LED was also measured and the angular intensity is presented in figure 5.12, and the measurement values in table 5.4.

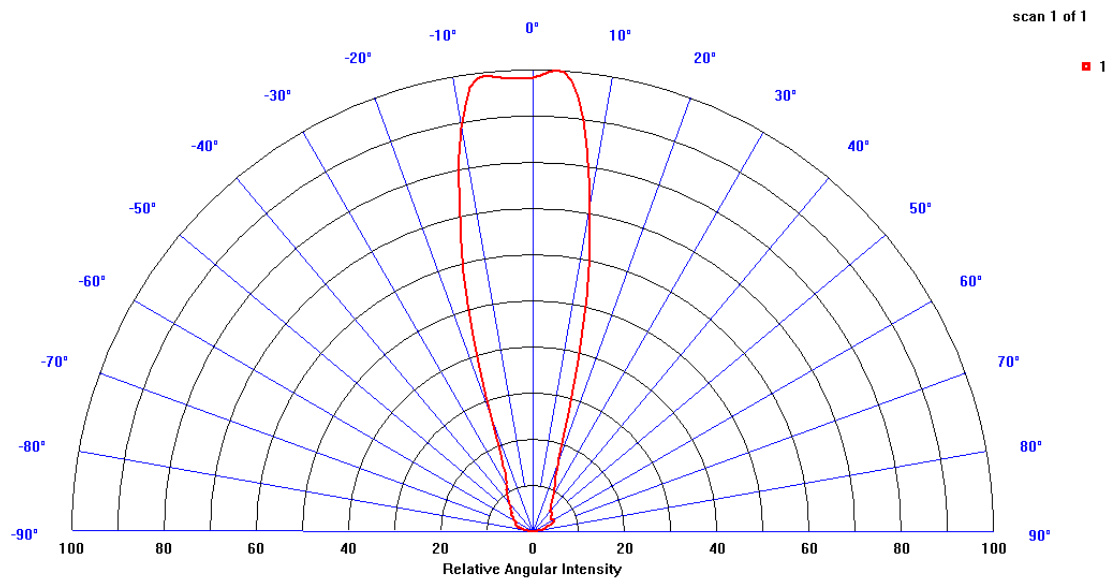


Figure 5.12. Angular intensity of the LED with dome-type lens.

Table 5.4. Measurement results.

	Luminous flux / mlm	Luminous intensity / mcd	Collimation angle / °
Manufacturer's lens LED	405	793	29

As can be seen, the collimation angle and intensity value are better than earlier, but one cannot say that these results are unattainable for diffractive optics. Although the luminous flux is not known for this LED before encapsulation, it can be assumed that the 405 mlm that was measured, is comparable with the results for DO lens LEDs. The big geometrical lens, whose RI is unknown and is probably lower than 1.57, seems to decrease the flux, which is obvious, due to the large volume of matter on the LED.

There are clear advantages to using a flat diffractive optics lens, rather than a geometrical lens. Because the geometrical lens is convex, further attaching the LED to another application may be difficult or even impossible. This problem does not exist with flat lenses. Additionally, fabrication costs are lower with DO lenses.

As a remark, the LED manufacturer also offers discrete collimation lenses that can be placed onto desired LEDs. These particular lenses are 10 mm thick, and provide a collimation angle value of 15° . Using the same kind of discrete DO lenses, as in the tests above, the same, or even better collimation angle value can be achieved with a lens that is only 250 μm thick. Additionally, the luminous flux of the LED is improved with DO lenses, due the fact that there are no large housings around the LED, as with the refractive lens.

6 Step hot embossing

In the previous chapter, the light sources were successfully collimated. When light is more collimated, coupling it to an application, such as a light guide is better and more efficient. However, in order to have comprehensive control over the light, one has to also have an efficient way to out-couple the light from a substrate. In this chapter, a technology known as step hot embossing will be introduced, and it will be shown that the technology is fully functional, allowing it to be used in several in-coupling – out-coupling applications to be presented later in this paper. This technology utilizes the tools that were fabricated in chapter 4.1.1.

Step hot embossing is a technology, where different kinds of structures are replicated by pressing them onto a material, usually onto a polymer. Pressing is performed mechanically, using precise pressure, temperature and time values. These *replication parameters* play a vital role in the success of step hot embossing. The word step comes from the fact that, unlike in conventional flatbed embossing, or in roll-to-roll embossing methods, the structures are embossed individually, by stepping them one after another. The structures may be macro-sized patterns, or microstructures. In this work, the blazed grating microstructure is used.

Step hot embossing also offers the possibility to use different types of structures during the same embossing process, because the structures used are on a tool, which can be changed to another during the process. Thus, the end-product may contain a heterogeneous amount of structures, which is an obvious advantage to existing

embossing methods. Additionally, step hot embossing allows a large surface area to be filled with microstructures, while maintaining good quality at macroscopic levels. The large area can then be replicated, as a whole, to a substrate to be used as a master for further large area replication processes. Depending on the manufacturing device, this technology can be also utilized in mass production. In this work, the Toray flip-chip bonder is an excellent production machine, at least for demonstration.

6.1 Embossing objectives

The success and quality of replication are the two most important issues when analysing the replica. The ideal situation would be when the replica is an exact mirror image of the original. This is, of course, very hard to achieve because there are several factors that affect quality - replication parameters, and their accuracy being top of the list. The material, on which the embossing is made, adds its own challenges to determining quality.

The primary focus is on the depth of the replicated structure, which controls the success of replication. The overall depth of the structure cannot be too low, nor can it be pressed too deep into the material. These two situations are depicted in figure 6.1 along with a successfully replicated structure.

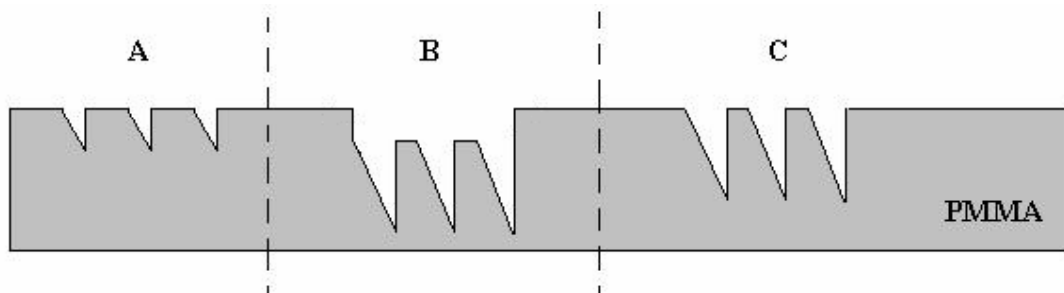


Figure 6.1. Three different ways in which replication may happen, with C being the objective.

The structure in figure 6.1 can be also called an output grating coupler, as the grating deflects the wave front progressing horizontally inside the substrate. Figure 6.2, on the other hand, shows a different type of a blazed grating.

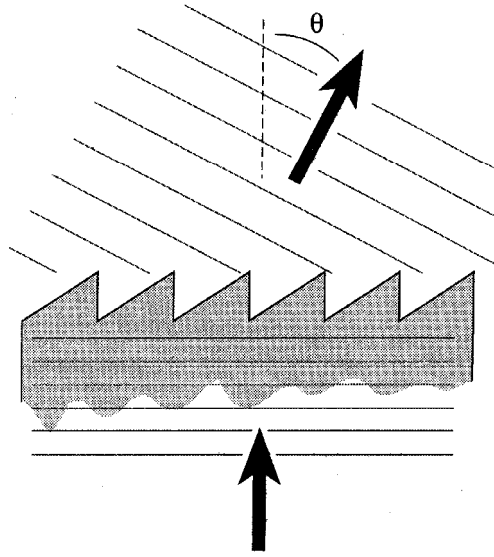


Figure 6.2. A transmissive blazed grating showing how the light deflects, as a result of the grating [5].

In order to redirect all the incident light power into one specific diffracted order, the wavelets deflected from all the facets have to form one, plane and continuous waveform. From this requirement, it can lead to an expression for the relief height h , of this grating [5, 22].

$$h = \frac{m\lambda}{n - \frac{\sqrt{p^2 - m^2\lambda^2}}{p}}, \quad (4)$$

where n is the refractive index of the substrate and p is the grating period of the relief. A blazed grating with relief height h , diffracts an incoming plane wave of wavelength λ into plane wave, yielding 100% diffraction efficiency in the desired m th diffraction order. If the relief height differs from the optimum height, the wavelets will not be perfectly phase-matched for the m th order, and other orders appear [5].

Figure 6.3 shows the diffraction efficiency in a few diffraction orders for an ideal continuous-phase transmissive blazed grating as a function of grating relief height. The relative height error is given as the difference between the actual height, and the

optimal height divided by the optimal height, where a relative height error of zero corresponds to the optimal height for the first ($m = +1$) diffraction order [5].

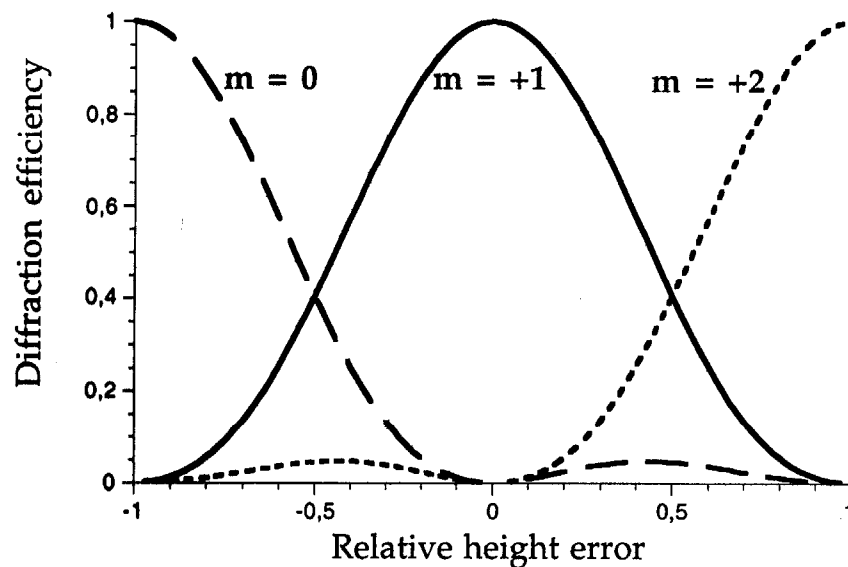


Figure 6.3. Calculated diffraction efficiencies in some orders for a blazed grating as a function of relative height error. A relative height error of zero corresponds to the optimal height for the first ($m = +1$) diffraction order [5].

It can be seen that the curve for the +1 order is relatively flat around the optimum height. If the requirement of the grating is that more than 90% of the diffracted power ends up in the +1 order, the relief height must not deviate more than $\pm 17\%$ from the optimum height [5]. Although this type of transmissive blazed grating is different to the situation in this thesis, the estimation of 17% will be used in this paper too.

If the relief height is sufficient, but the structure is pressed too deeply, as shown in figure 6.1B, a vertical wall will be formed around the replica. This area will not out-couple any light and the diffracted power will therefore decrease.

Another quality factor is material-dependant. All polymers that are used in this technology should be thermoplastics, as they do not show the so called memory effect - i.e. if they are processed above their glass transition temperature T_g , the form in which they are processed will remain, even after cooling. It is the polymer's mould shrinkage value and the smoothness of the formed surface that affect the quality. If

the surface is rough, light will scatter from it, and the coupling effect will not happen so efficiently. The value of mould shrinkage should be as low as possible.

6.2 Success of replication

To demonstrate the success of step hot embossing, two sets of tests were performed. In both sets, three temperatures, 80 °C, 100 °C and 120 °C were used. During each temperature, seven embossing were conducted with increasing pressures, from 3 N to 15 N. 21 embossing were performed in one test period in total. These were done with the two tools, which were introduced in chapter 4.1.1. The replication time was kept at a constant 10 s, because its effect on the replication was calculated to be more negligible than the two other parameters', temperature's and pressure's. It also ensured that the whole test process was more understandable and controllable. The base material in both cases was 0.5 mm thick PMMA. With visible light transmission being 92% and mould shrinkage low, PMMA was a good choice for the demonstration. The analyses of the replicas were performed using a confocal microscope, as it provided a 3-D scanning mode, allowing cross-sectional images along with an accurate vertical and horizontal measuring.

6.2.1 Preparations for analyses

Measuring the structures made with tool A was done without any problems, but the second tool was more troublesome. Tool A had been more in use, so the structure had been slightly flattened from the top, as can be seen in figure 6.4. The flat peaks replicated as planes, which allowed the scans for the tool A replicas, because the microscope light reflected from the plane valley back to the microscope, giving a proper response.

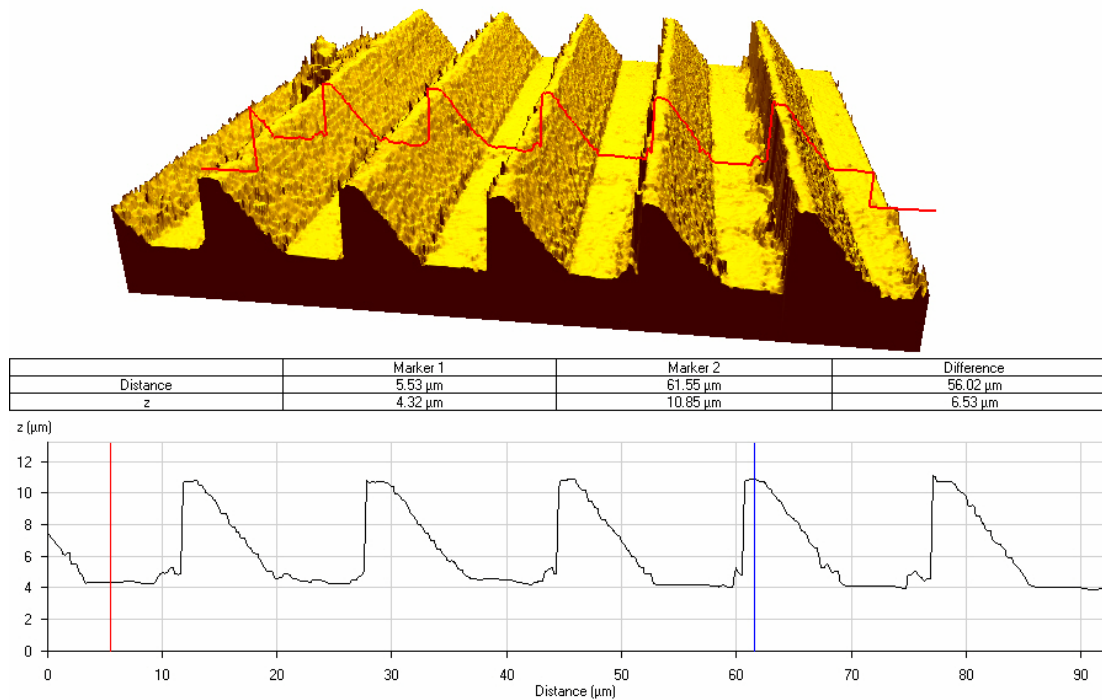


Figure 6.4. A confocal scan of tool A showing its blunt peaks.

The second tool had sharper structures, and hence replicated very sharp valleys. Due to the optical nature of the structure, the bottom of each replicated valleys could not be seen. This was because the microscope light scattered away at those points. Making silicone replicas of the replicated tool B structures solved this dilemma. Silicone is very good for replicating microstructures because it has low flow properties and its surface tensions are low, which enables it to fill all structures, even at sub-micron levels. This allowed the scanning over the silicone double replicas to succeed.

Silicone replication is in fact, an exquisite way to demonstrate the success of step hot embossing. It also makes measuring with a scanning electron microscope or profilometer redundant. SEM does not allow measuring in a vertical direction. As a result of the large amount of samples that need to be prepared, the whole process becomes expensive. Sample preparation takes time, and cross-sectional images can be obtained from one point only. Profilometer and atomic force microscopes are accurate, but this kind of serrate profile used is too difficult for them to measure. Using silicone, a very precise replica is obtained from the whole area of interest. It is also cheap, and all kinds of upright structures can then be measured with a confocal microscope. All this can be done at room temperature. Detaching the silicone from the

base material is easy because silicone adheres very little. As no sample preparation is required, cutting the structure in desired sections allows authentic cross-sectional images to be readily obtained.

To recapitulate, the scans of tool A replicas were, in reality, structure depth measurements straight from the replica, while the tool B replica scans were height measurements from the double replica. However, this gives the real structure depth values in the first replica too.

6.2.2 Analysing methods

Each embossed area was scanned at five different locations using 1000x magnification, the scanning area being 90 x 90 μm . Within each scanning point, 10 measurement lines were taken, covering the whole scanning area. Figure 6.5 shows the scanning points and in figure 6.6 one scanning area is shown in more detail.

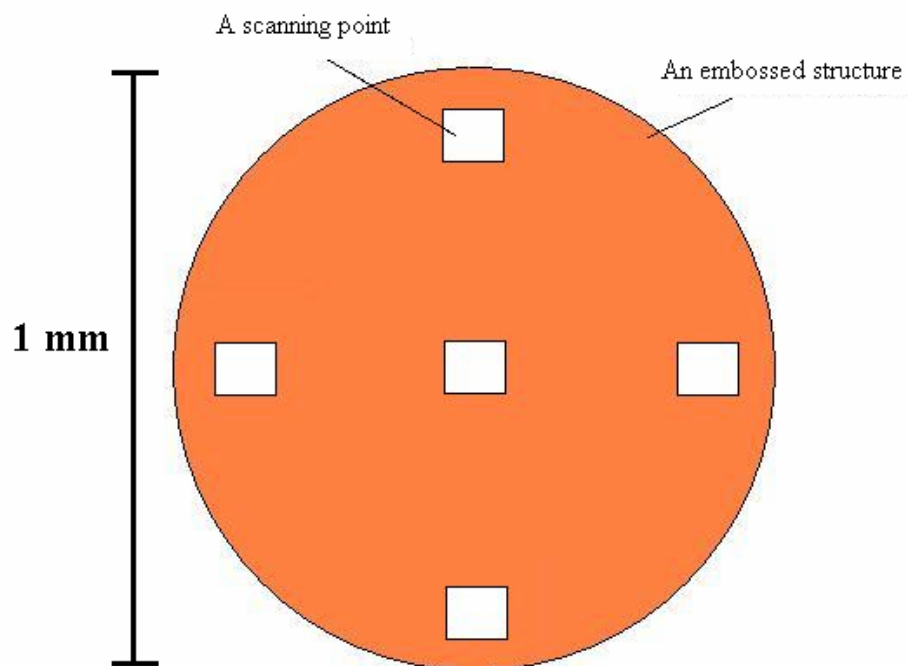


Figure 6.5. One embossed structure with the five scanning points.

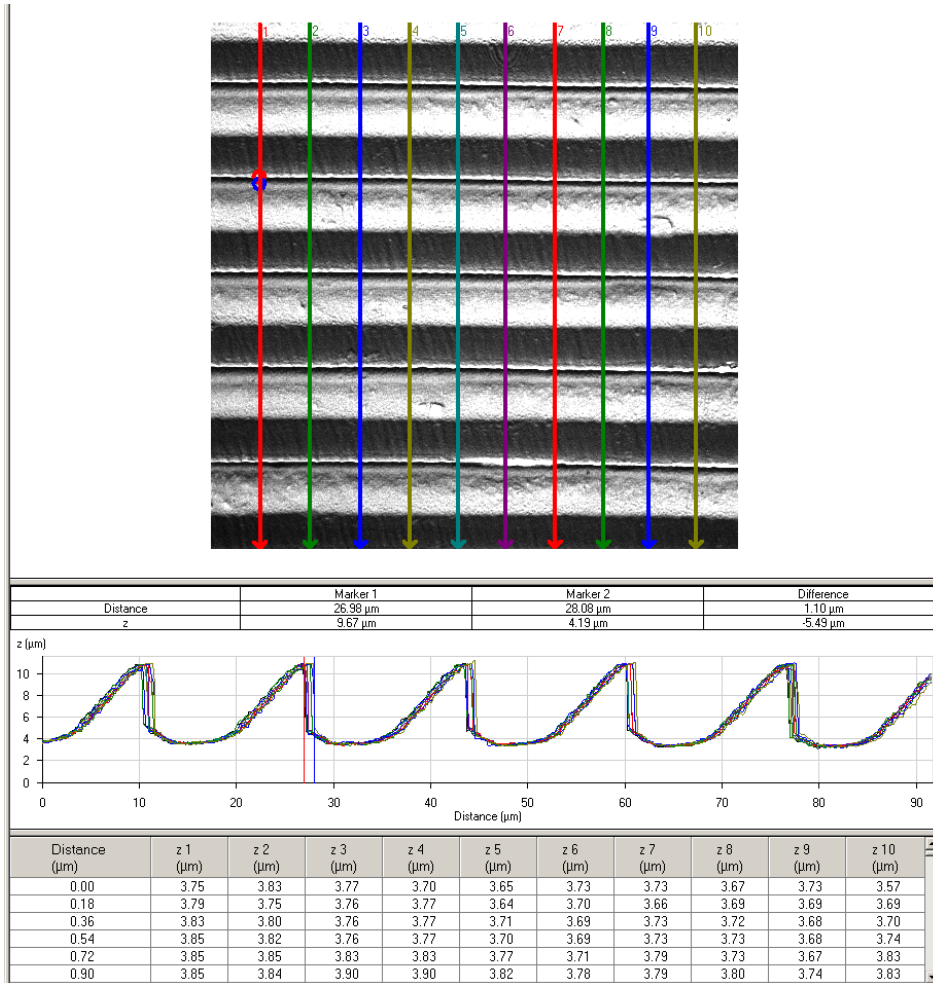


Figure 6.6. One scanning area showing the ten measurement lines whose values are in the table below the profile.

In figure 6.6 the structure used is one of the silicone replicas. However, the following analysing methods are applicable to the replicas made with tool A, only reversed due to reversed structure direction. The values in the table in figure 6.6 can be exported to Excel, for example, for statistical analyses.

The main focus is in the overall structure height in each embossed area. It is calculated as an average of the five scanning points shown in figure 6.5. To obtain the mean structure height within one scanning point, the average height from the ten measurement lines were calculated. To have the average from the ten measurement lines, a mode, which is the most frequently appearing value, was first retrieved from a table like in figure 6.6. The mode value represents the mean bottom point of the structure within the scanning point. Next, the average location of the structure top in a

scanning point had to be solved. For this, each of the ten columns were sorted in descending order to place the highest measurement values at the top of the data set.

The two markers in figure 6.6 are placed at about 1 μm distance from each other, which is a good estimate for a width of a peak. As can be seen in figure 6.6, the z_i values are taken at 0.18 μm intervals, which means that if the seven highest values ($7 \times 0.18 \mu\text{m} = 1.26 \mu\text{m}$) from each of the ten columns are retrieved and an average calculated from those, the location of the average structure top is obtained. The mode value is then extracted from the structure top average, thus giving the mean structure height within one scanning point. Finally, the overall average is calculated from the five scanning points. Both tools were likewise scanned and analysed.

Each scanning point also produced a standard deviation. To represent a standard deviation that reflects the standard deviation of the entire embossed surface area, equation (5) was used [11].

$$\text{STD} = \sqrt{\frac{\sum_{i=1}^n \delta_i}{n^2}}, \quad (5)$$

where δ_i is the mean square deviation of each scanning point and n is 5 in this case.

6.2.3 Test results

The results of the tests are presented in tables 6.1 and 6.2 for tools A and B, respectively. Graphs from these are also presented.

Table 6.1. Results from the test conducted with tool A.

Temperature / °C	Average structure depth / μm						
80	0.4	1.0	1.8	2.1	2.1	2.5	2.7
100	1.3	4.1	4.4	6.0	6.2	6.4	6.8
120	6.2	6.8	7.0	6.5	6.8	6.7	6.9
Pressure / N	3	5	7	9	11	13	15

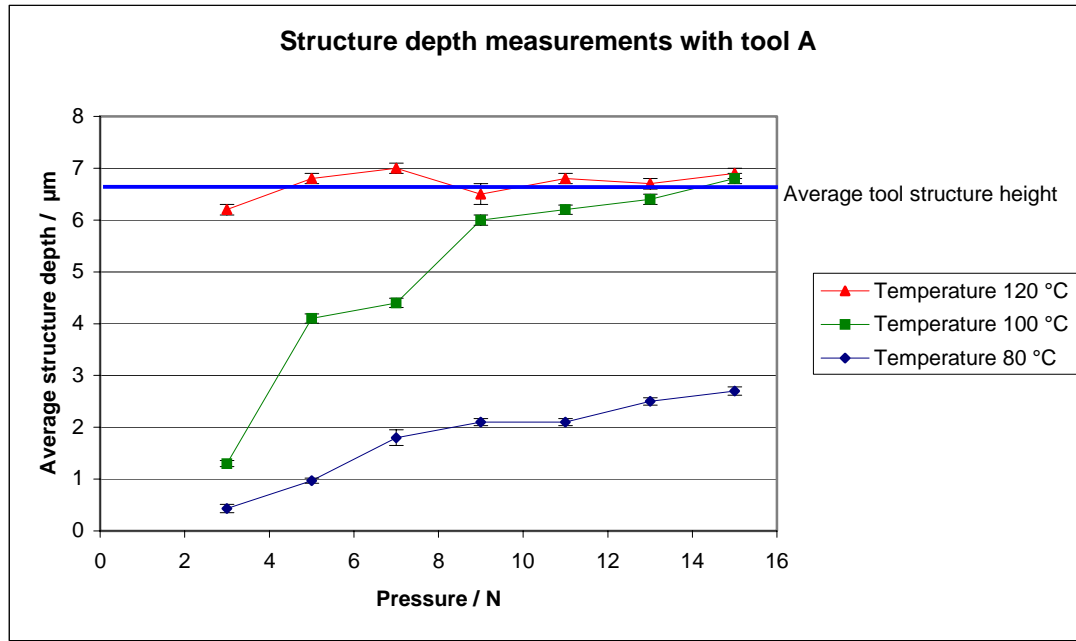


Figure 6.7. Graphs from table 6.1. Average tool structure height is 6.7 μm .

Table 6.2. Results from the test conducted with tool B.

Temperature / °C	Average structure depth / μm						
80	2.5	4.0	4.7	5.6	6.5	5.8	5.9
100	3.1	7.1	7.4	7.3	7.3	7.5	7.3
120	7.6	7.3	7.3	7.3	7.1	7.5	7.2
Pressure / N	3	5	7	9	11	13	15

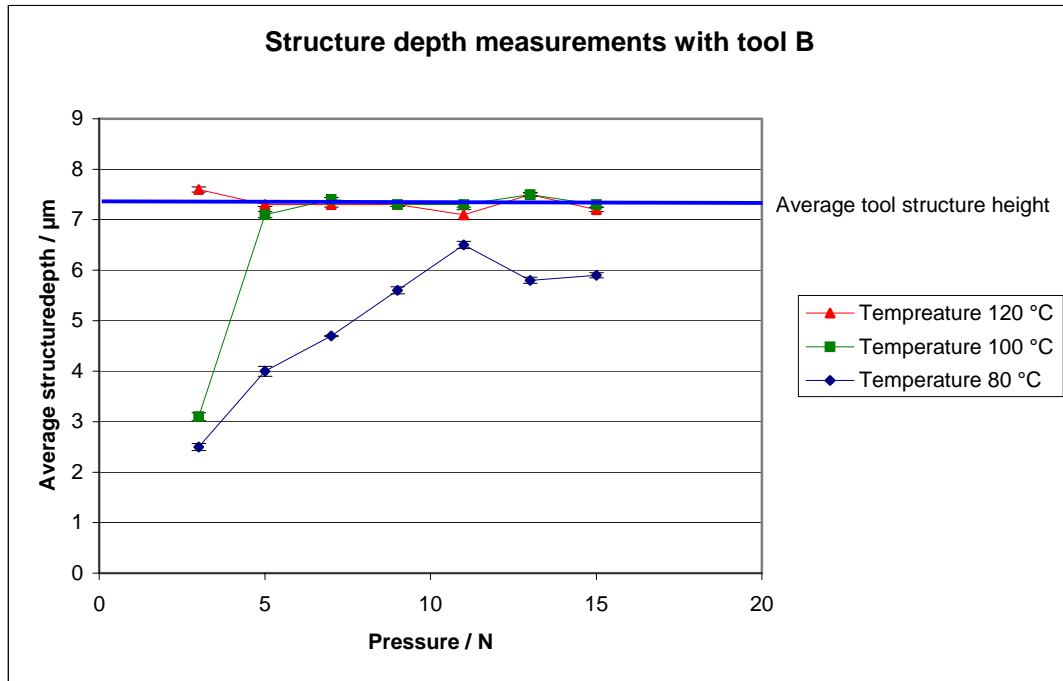


Figure 6.8. Graphs from table 6.2. Average tool structure height is 7.4 µm.

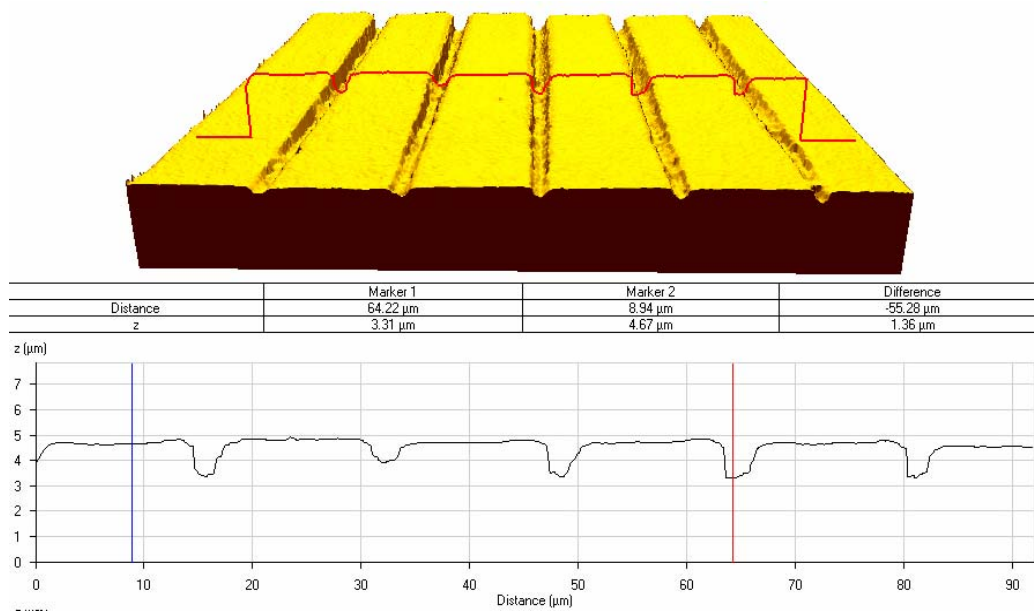
By looking at the diagrams in figures 6.7 and 6.8 one can find both similarities and differences. It is expected that an increase in pressure at constant temperature increases the embossed structure depth. Also, an increase in temperature at constant pressure increases the embossed structure depth. Although there is some variation, these assumptions hold, and this is shown in figure 6.9. There is, however, a distinct difference in the dynamic range of the diagrams between the two tests. As the peaks are quite blunt on tool A, it is obvious that at low pressures and temperatures, the structure depths are also low, compared to tool B in the same circumstances whose peaks on the structure are sharp.

It is also clear in figure 6.7 that by using 100 °C, the control of the structure depth over the whole scale is the best. This is understandable because the T_g value for bulk PMMA is 105 °C [12]. Although in figure 6.8 the diagrams are not so distinct, it is the 100 °C curve that has the most rapid increase in depth, and thus, the curve easily reaches the “ideal” structure depth.

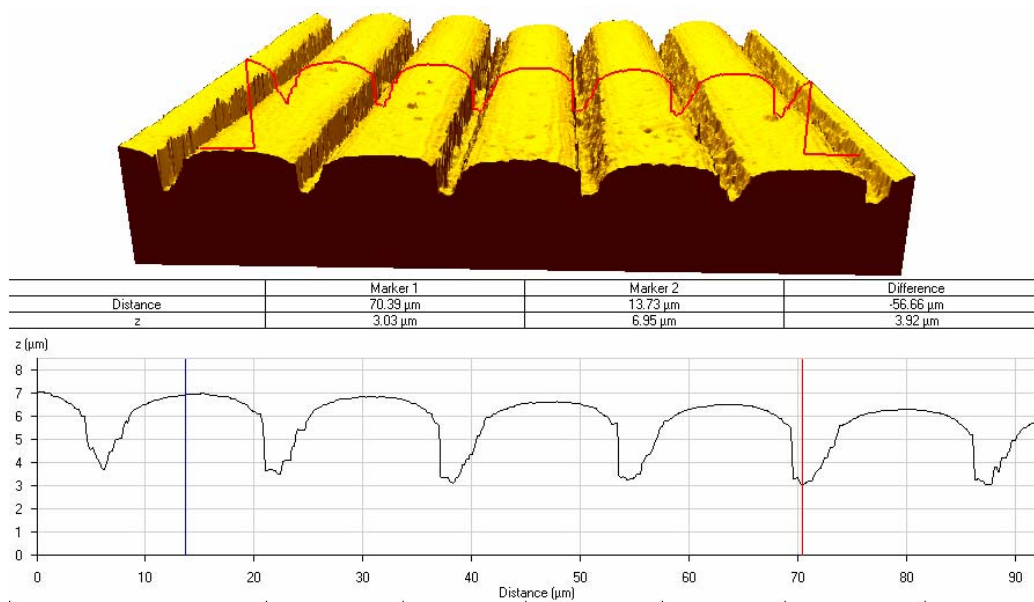
In figure 6.9 are three pictures of replicated structures made with tool A. In figure A the temperature is 80 °C, in B 100 °C and in C 120 °C. The pressure is 7 N in all

cases. It is evident how the depth of the structures in a replica increases with temperature. There is also interference in figure C, coming from the measuring system. The interference can be seen as sharp spikes on the oblique side of the structure profile. They are formed because the microscope has not received a response from those points due to light scattering. It is possible to filter the interference in the measuring software, but too much filtering also alters the result.

A



B



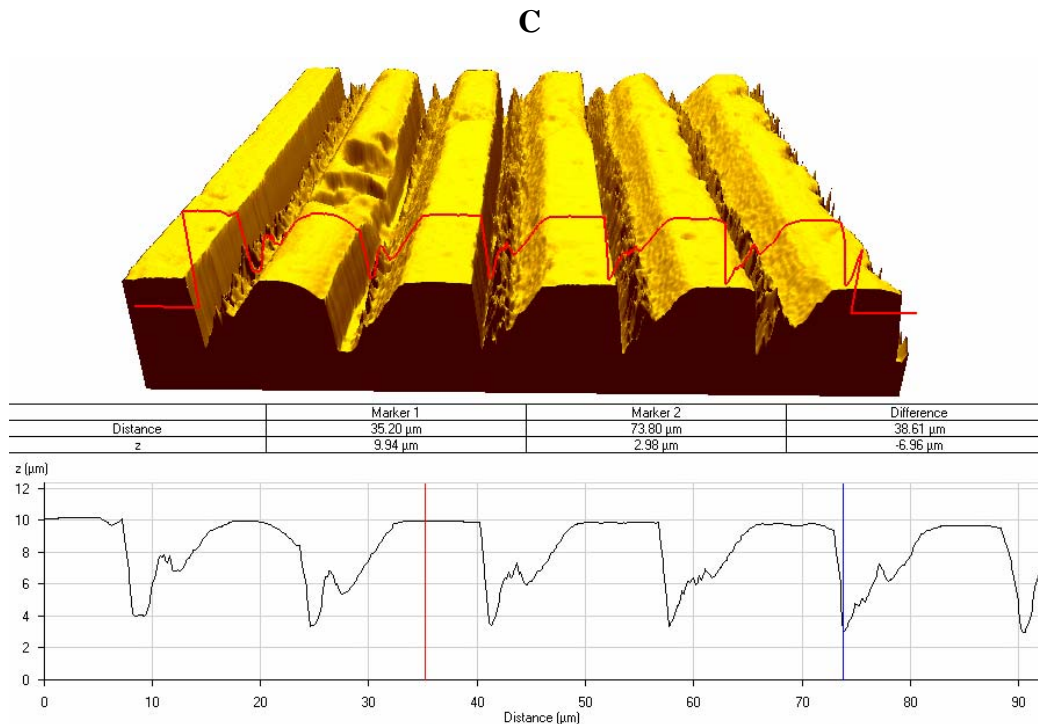


Figure 6.9. Structure depths at increasing temperatures at a constant pressure. In figure **A** the temperature is 80 °C, in **B** it is 100 °C and in **C** it is 120 °C. Pressure is 7 N.

A replica can never be better than the master, from which it was created. Consequently, if a replica of a replica has almost as good structure profile as the master element, it proves unambiguously, that replication by step hot embossing works. In figure 6.10 a silicone replica scan and a tool B scan are presented. It shows how good the silicone replica is, compared to the master.

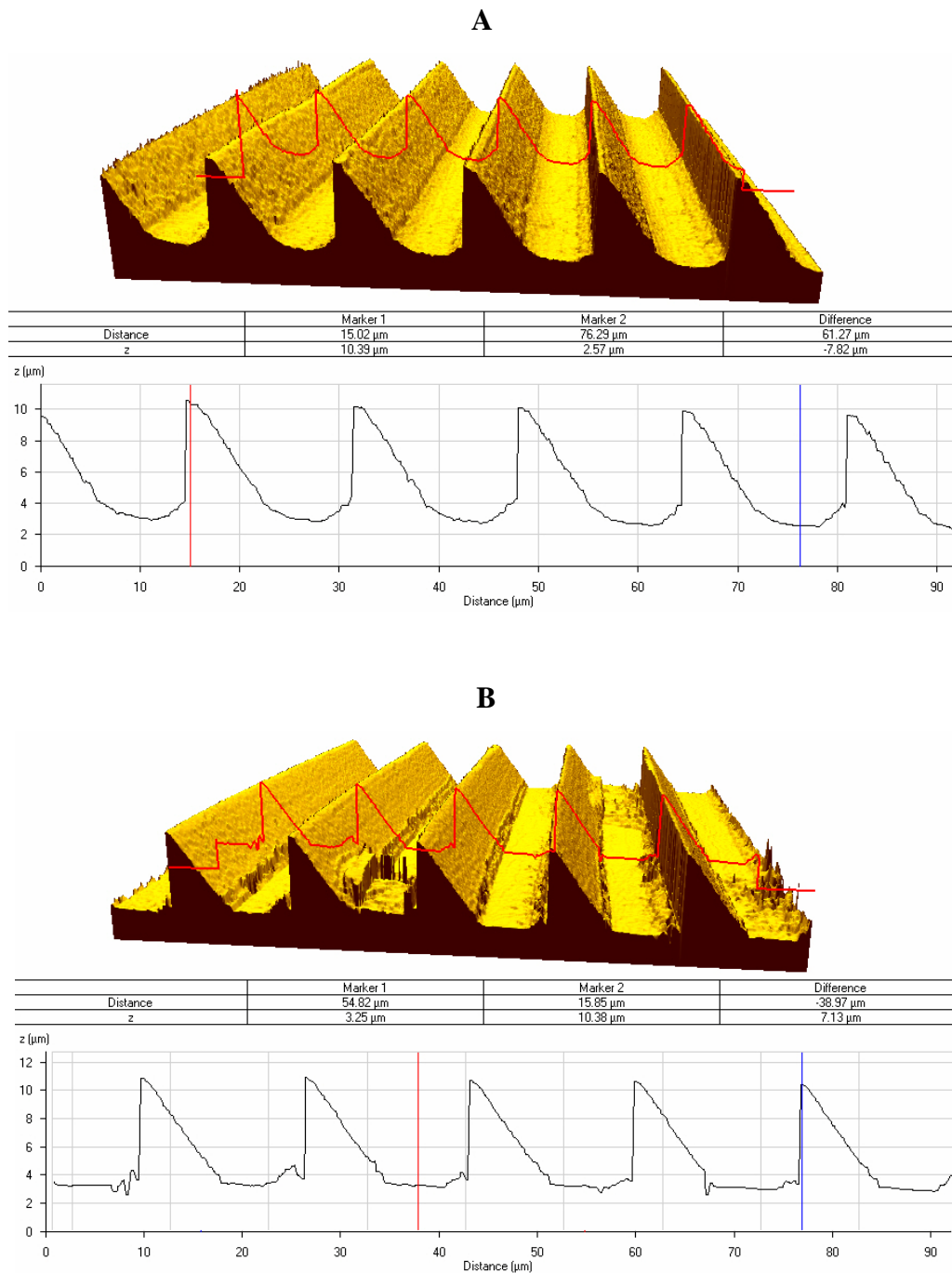


Figure 6.10. Comparison between a double replica **A** and the master **B**.

Although there is some minor rounding on the bottom of the silicone replica (on the top of the first replica), it is safe to say at this point, that the step hot embossing technology presented here is a workable method. It is now simply about finding the ideal replication parameters to achieve the best quality.

6.3 Quality of replication

In the section where the tools were presented, the meanings of differences between the tools were left unclear. It is assumed that by using tool type A, the large surface area around the tip will get in contact with the material during embossing, physically preventing the structure from being pressed too deeply into the material, thus making this tool type self-limiting and independent from used upper pressure. After a few preliminary tests, however, it became clear that as a result of the high temperature, the large contact area deformed the material around the replicated structure. It was decided that tool type B should be fabricated. The substantial difference between the structure top and the rest of the tool should ensure that only the structure area being embossed was in contact with the material. For this type, the assumption, on the other hand, was that the structure being pressed below the polymer's surface, as shown in figure 6.1B.

Next, it would be prudent to study whether the assumptions related to the tools apply, and how deeply the structures are pressed into the material in the tests, and could there be found some replication parameters that appear as the best choices, when aiming towards replica shown in figure 6.1C. As mentioned earlier in this chapter, if the requirement for diffracted power is more than 90%, the relief height must not deviate more than $\pm 17\%$. By looking at tables 6.1 and 6.2, one can immediately eliminate all the pressure and temperature values that gave structure depths lower than 83%, from the average tool structure heights. This leaves all the values from row 120 °C for both the tools, the last four values from row 100 °C for tool A, and the last six values from row 100 °C for tool B, to be studied further.

6.3.1 Analysing methods

Measurements were again performed with confocal microscope, only this time, measurements were taken at the edges of the embossed structures from four measuring points, leaving out the centre measuring point. The measurement points are shown in figure 6.11. Within each of the four measuring points, six measurement lines were taken over the edges of the embossed area. The reason for six measurement lines instead of 10, as before, will be explained later. It was now possible to take the

measurements directly from the replicas, because the measurements were done from the surface of the polymer to the top of the structure, thus negating the need for silicone.

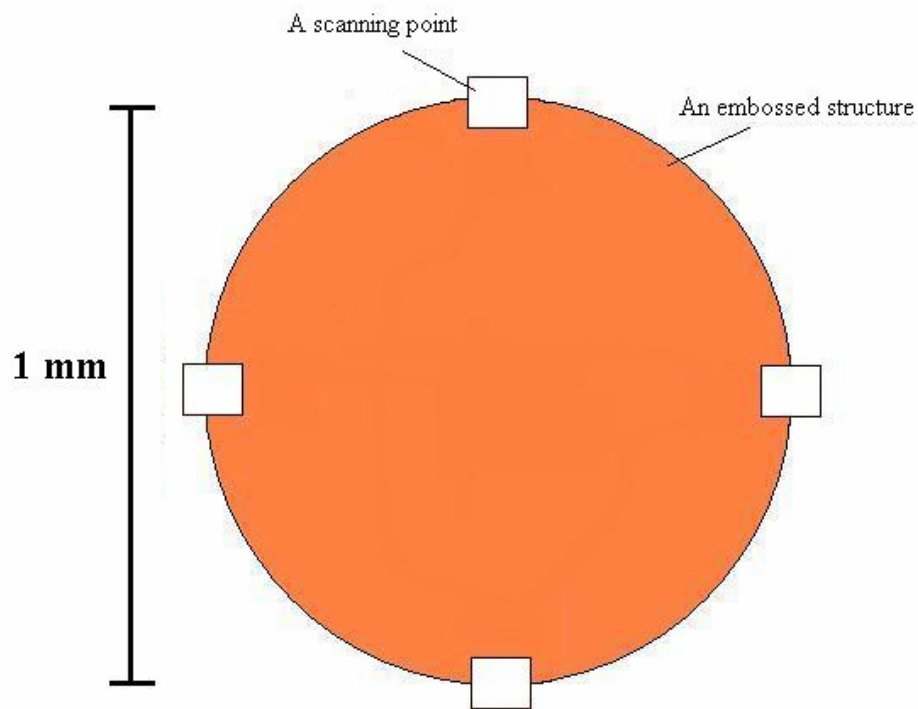


Figure 6.11. The four scanning points.

The basic analysing methods were the same as before, meaning that the average depth of how deep a replica had been pressed was calculated as an average of the four measuring points. However, to obtain the mean difference between the surface of the polymer and the structure top, within a scanning point, was not so straightforward in this case. The methods used were not the same for each scanning point. The “north” and “south” measuring points are comparable to each other, as were the “west” and “east” points. However, “north” and “east” points, for example, are not comparable to each other, and this is explained more clearly in figure 6.12, which shows two scan line results obtained from the two locations. Figure A was obtained from the “north” measuring point, and B was obtained from the “east” measuring point. Both are from the same replica, and the axis values are arbitrary units.

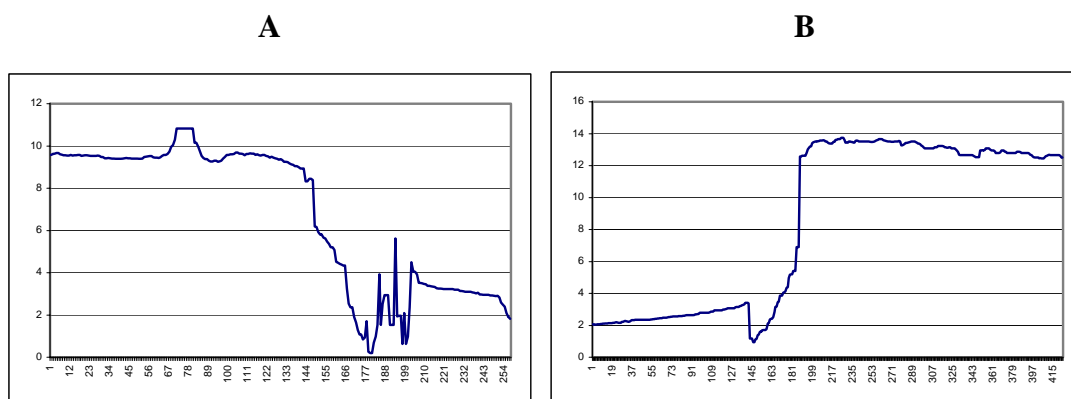


Figure 6.12. Two scan lines obtained from different locations on the replica.

In both cases, the height of the step was calculated, but due to the interference in figure A and reversed profiles, the same methods could not be used for both. Interference was created in most of the “north” and “south” measuring points, because the microstructures at these points were orthogonal to the measuring lines. The reason for the interference is explained by the measuring procedure, as measurements were only performed from the top of the polymer to the top of the structure, with the valleys left unmeasured. In the “west” and “east” points, as in figure B, interference was not produced, because the measuring lines were drawn along the structure tops and no crossing over unmeasured valleys had to be done. These are just few examples of why individual analysis had to be used.

The height differences in figure 6.12 were calculated by first retrieving the mode value from the measurement data for both A and B – the mode was settled somewhere on the polymer surface, because majority of the response was received from that area. The average location of the structure top was then calculated separately for figures A and B. In A, the average was retrieved from the last few data values at the end of the data set, whereas in B it was retrieved at the beginning of the data set. The step height was then obtained by extracting the average from the mode. To reiterate, the lines in figure A and B is only one of the total of six, but the treatment above can naturally apply to all six lines at the same time.

6.3.2 Results of replication quality

The results of this study were not what were expected. For instance, the assumption of over pressed structures with tool type B is not valid. As can be seen in figure 6.13, the replicated structure is on the same level as the polymer surface - and this applies to all parameter values measured. However, replication with this tool forms burrs on the fringes of the structures, which is a problem when embossing these structures side by side. It is obvious, that by pressing the structures onto the polymer, the material has to go somewhere from those areas, and in this case, burrs are formed. The burr heights for different replication parameters are presented in table 6.3 and they are measured as an average over the four measuring points. Figure 6.13 also shows the reason for the issue of six measurement lines, as discussed earlier. Only six adjacent structure tops fit inside the scanning area.

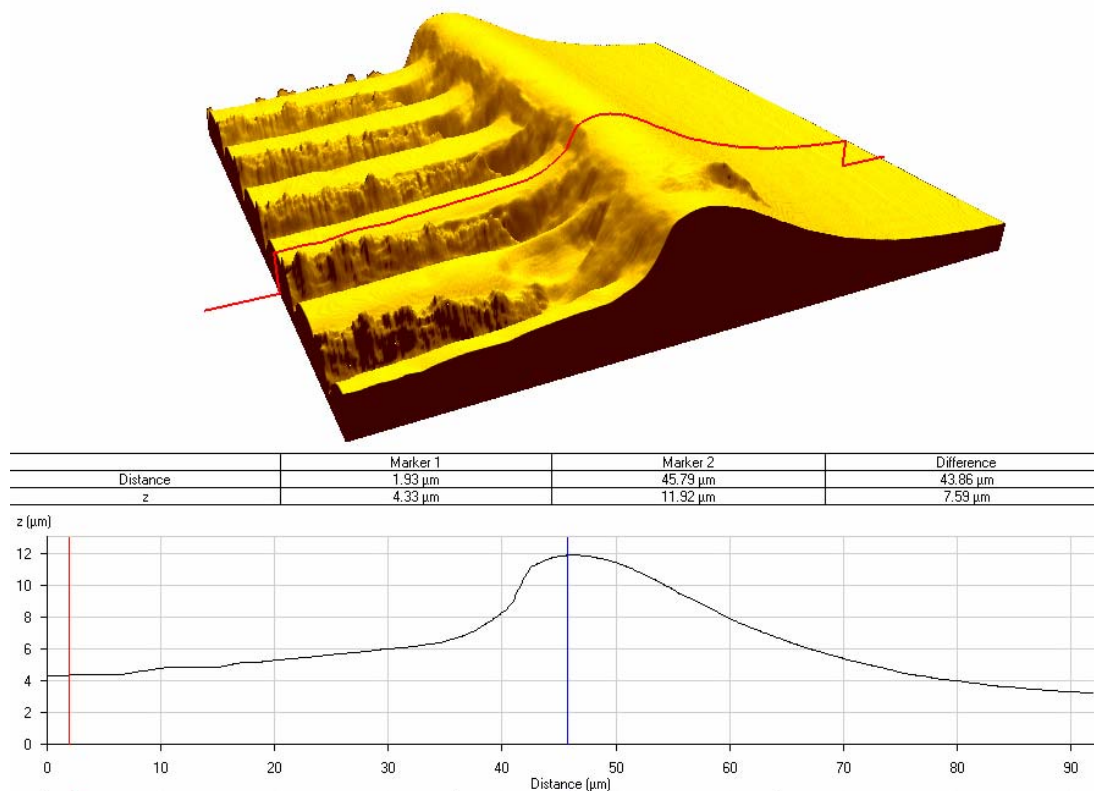


Figure 6.13. Tool type B creates burrs around the replica.

Table 6.3. Burr heights in tool B test.

Temperature / °C	Burr heights / μm						
100	-	0.3	0.5	1.1	1.4	1.1	1.0
120	2.7	4.1	4.5	6.1	6.2	5.5	6.2
Pressure / N	3	5	7	9	11	13	15

The results are apparent. The burr heights are only tolerable in seven cases, where the values are under 3 μm . Furthermore, the height of a burr seems to increase more with temperature, rather than with pressure. This is explained by the viscosity of the polymer, which decreases along with rising temperatures. The tool was not perfectly perpendicular, which caused a variation between the four measurement points. The burr heights at the “east” measuring points were greater than in the other three.

The results for tool type A also conflicted slightly with expectations. Both of the tools were hand made and far from ideal, as the fabrication methods were quite rough, which means that although the tip in tool A should have been only about 7 microns high, in reality there was an additional 10 micron gap between the contact area and the bottom of the structure. Figure 6.14 shows how the surface of the polymer is smooth due to the contact area, as assumed, but the structure itself has formed below the polymer surface as a result of the gap. In all cases where the contact area was in contact with the surface, it made the surface smooth. The results of these steps are presented in table 6.4.

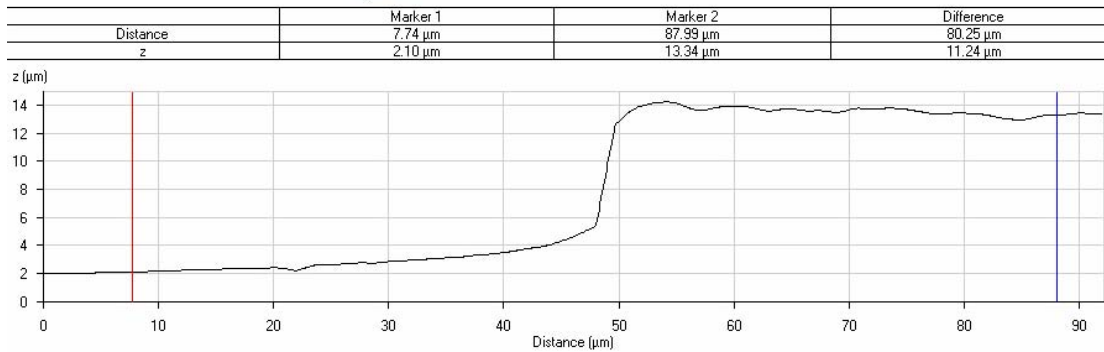
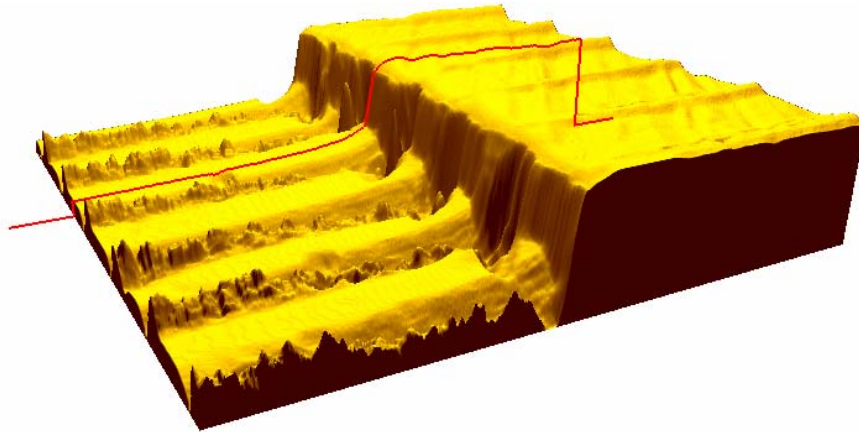


Figure 6.14. Even a small gap between the contact area and the bottom of the structure on tool type A caused a step.

Table 6.4. Step heights in tool A test.

Temperature / °C	Step heights / μm						
100	-	-	-	1.4	0.9	1.2	3.2
120	1.3	3.6	11.0	10.2	11.6	11.7	11.4
Comment	A burr and a step						
Pressure / N	3	5	7	9	11	13	15

There was some variation in these results, which is why a comment row has been added to the table. With the lower temperature, the results are a variation of the polymer surface, or minor steps. With the higher temperature there was one case with a 9 N pressure where the replica had both a step and a burr – a step was formed at the “east” measuring point and a burr at the “west” point. This was due to the lack of perpendicularity of the tool. Again, the step heights seemed to increase with temperature, which caused the decrease in viscosity. The results, however, were quite promising when thinking the assumption that the tool could work as a self-limiting and being independent of used upper pressure.

6.4 Conclusions for step hot embossing

There are both pros and cons for the two tool types. Tool B seems to always form the replicas on the surface of the polymer, but burrs are also formed. Tool A does not form burrs, but the contact area on the tool must be on the same level as the bottom of the structure. This sets high demands on the fabrication of this tool type. However, the results indicate that this self-limiting assembly could work, which would make the upper pressure value negligible. If the contact area on the tool was an effective insulator, like Teflon, for example, it could be possible to replicate almost ideal structures because no deformation of the surrounding material due to heat would exist. One has to remember, though, that if the contact area on the tool was large, meaning over ten millimetres in diameter, and because perpendicularity is peremptory, the base material's surface must be very smooth and there can be no variation. The same requirement applies to the possible insulator.

To conclude the analyses of replicas and tools, table 6.5 presents the replication parameters for the tools that should be used in this step hot embossing process, in order to achieve a replica that fits inside the requirement window. Based on the results for the tools, it seems that if an ideal tool could be fabricated, tool type A should be the one used. Because the T_g value for PMMA is 105 °C, it is obvious that 100 °C stands out as the best temperature value. The best outcome for the replica is achieved using a pressure higher than 10 N.

Table 6.5. Recommended replication parameters for both of the tools.

Temperature / °C		Pressure / N		
100	9	11	13	15
120	3	-	-	-

All the results that are gained are, of course, limited to the area of the replicated structure. In these cases, the area was $\sim 0.8 \text{ mm}^2$, but replicating larger areas will require more pressure and perhaps, a higher temperature, and vice versa.

Finding the optimal tool type, replication parameters and materials to achieve a replica like in figure 6.1C was an important aspect in this work. The reproducibility of

replicas, however, is a major factor when considering production, for example. Although the replication methods presented in this thesis are not bound to any specific production machine, it is worth knowing the limitations and abilities of the Toray flip-chip bonder, in order to be more capable of making an analysis of results gained from the bonder. The accuracy of the replication parameters controls the reproducibility. Knowing that the accuracy for pressure is ± 0.1 N and for temperature ± 1 °C, one can say that this machine is precise enough, when thinking in percentage values. For example, 0.1 N in a 3 N process is 3.3% and in a 15 N process, only 0.7%. Taking the worst case scenario, and based on the depth measurement results that are in the tables 6.1 and 6.2, a variation of 3.3% in pressure deviates the relief depths a lot less than 17%, which was the maximum allowed relief depth deviation.

6.5 Optical functionality of step hot embossing

Finally, to show that this kind of replication also works optically, a sample of binary light guide is presented in figure 6.15. The light guide contains a light out-coupling nanostructure as shown in figure 3.2. On the light guide, there are also embossed letters 'DI', which consist of multiple embossed microstructures. The light guide is illuminated by four white LEDs from the left side of the light guide. As can be seen from the picture, there is a huge difference in contrast between the letters and the background – the letters can be read clearly, even though the light guide itself is a light out-coupler. This feature enables the light guide to be utilized, for example, in the focused illumination of keypads in hand held devices. The contrast would be even greater if a pure PMMA was used, because pure PMMA does not out-couple light. However, a light guide was chosen for this because the existing nanostructure enables uniform illumination and light out-coupling from the whole surface area, thus making the shown embossing effect also better and more uniform.

To give some numerical values of the functionality, the light guide and the replicas were optically measured from eleven different locations. It is customary to use a nine-point measuring system for measuring light panels, but it was decided that eleven would be used in this case, in order to cover the letters. Figure 6.16, on the other hand, shows the intensity distribution of the light on the light guide more visually.

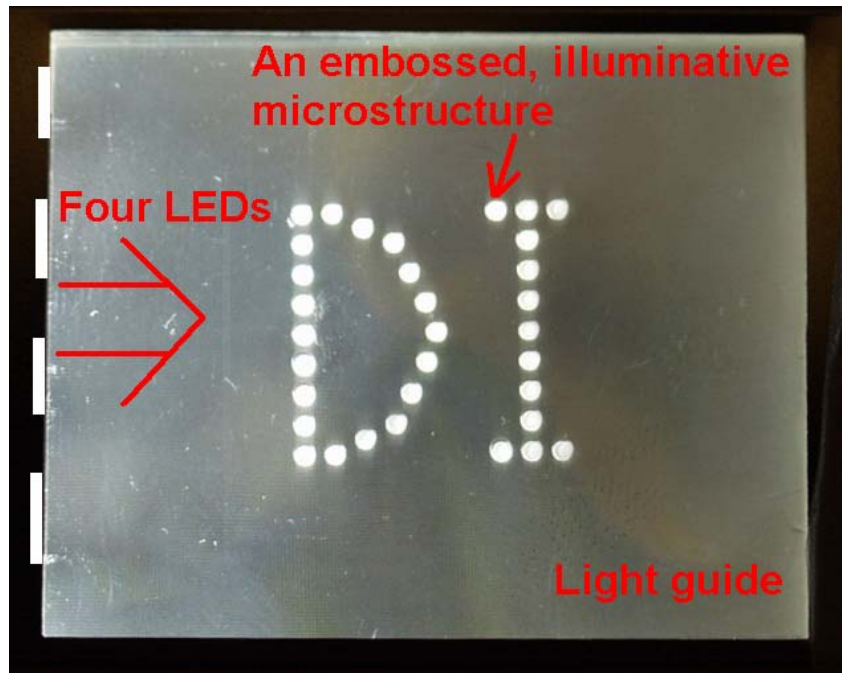


Figure 6.15. A light guide illuminated with four white LEDs from the left. Embossed blazed grating microstructures create the letters 'DI'.

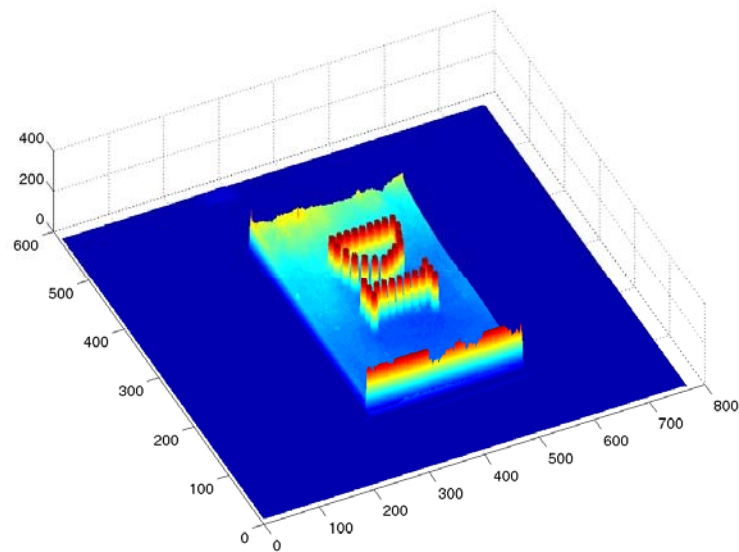


Figure 6.16. The light intensity distribution on the light guide. The axis values are relative.

Figure 6.17 shows the locations where the optical measurements were done on the light guide and the structures.

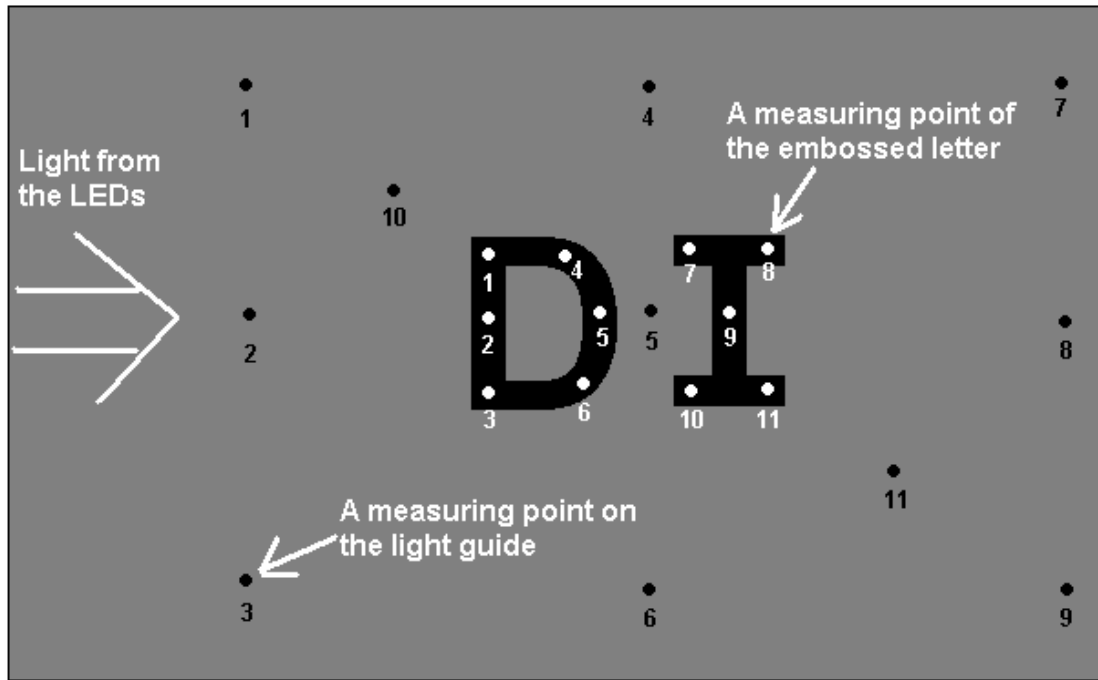


Figure 6.17. Measuring points of the light guide and the embossed structures.

Table 6.6 shows the measurement values for both cases. An average is also presented, to enable comparison between the replicas and the background. At this point, there is no doubt about the optical functionality of step hot embossing. The difference in luminance is quite remarkable, with the embossed structures showing an average luminance of over 795% higher than the light guide. The fact that the light guide itself is a light out-coupler, almost 800% increase from the luminance of the light guide really shows the potential of embossed microstructures.

Table 6.6. Measurement results from the light guide and microstructures.

Measuring point	Luminance / cd/m ²	
	Light guide	Embossed structure
1	687	5600
2	661	4990
3	592	3930
4	409	4360
5	291	3380
6	356	4770
7	363	3130
8	272	1900
9	312	1890
10	547	2530
11	273	1430
Average	433	3446
Difference		3013

The large deviation in the measurement values for the embossed structures is explained with the direction of the blazed grating patterns in an embossed area. All the microstructures in this example were embossed in such a way, that the blazed grating lines in the embossed areas were orthogonal to the in-coupled light, thus blazing the maximum amount of light out. As a result, the amount of light decreases rapidly behind an embossed structure, leaving very little light power for a structure behind the first one. However, if the swing angle of the embossed structure were adjusted in such a way, that the blazed grating surface area was smaller for the structures closer to the LEDs, than for the structures further from the LEDs, the decrease in light power could be reduced and the uniformity of light improved.

Another target for embossed microstructures is illustrated in figure 6.18. It shows how the microstructures could be embossed on a substrate for use in large backlight panels.

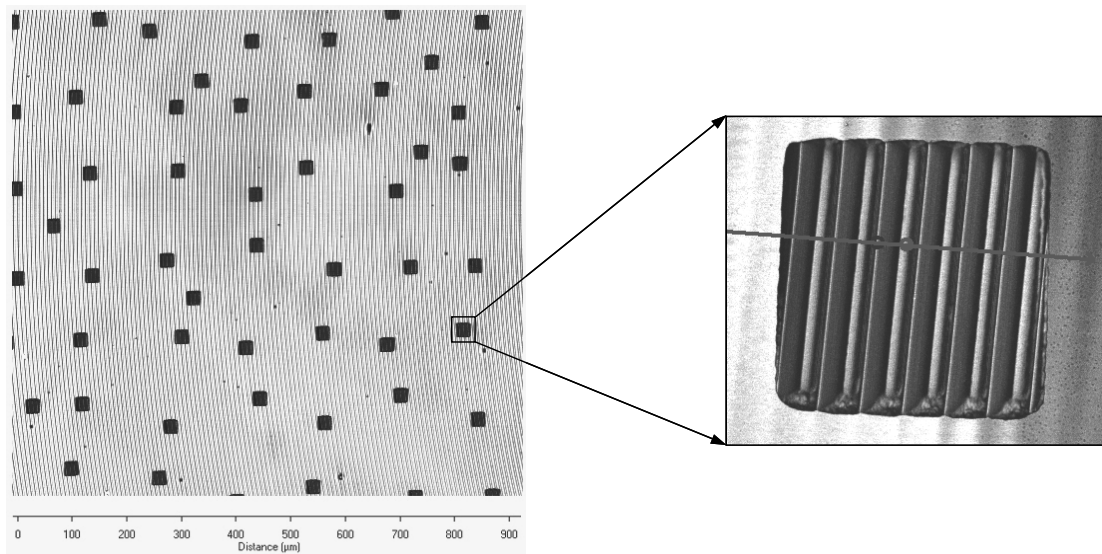


Figure 6.18. Asymmetric placement of embossed structures allows uniform light out-coupling [13].

Placing the structures asymmetrically, and modulating the structure density (patterned area vs. unpatterned area) on a surface, uniformity of light will be increased. Earlier in the chapter, it was mentioned that step hot embossing enables multiple structures to be used. Filling a surface with different kinds of structures and by modulating the structure density, asymmetric placement and the swing angle of the structures in such a way, that more light is out-coupled in the distance to the in-coupling LEDs, an

ultimate control of the uniformity of light can be obtained, and the number of used LEDs can be reduced. By using LEDs with diffractive optics lenses on them, the coupling of the light into these light panels is considerably increased, and thus, more light is obtained.

7 Wafer level replication

The third object of replication introduced in this thesis is a highly novel and sophisticated procedure, where the replication of micro- and nanostructures are performed at wafer level. The process has many different names, of which the most common are step imprinting or nanoimprint lithography, NIL. In the NIL process, a UV or thermally curable polymer resin is spin-coated on a wafer and the tool containing the structure is pressed into the desired areas. The polymer is then cured thus replicating the structure. Using only a few process steps, the replicated structure can then be transferred onto the substrate. NIL is thus, typically used to replace the old photolithography methods that suffer from alignment problems and a huge amount of process steps. As can be seen here, the NIL process is similar to the embossing process presented earlier. Typically, in the field of optics, where different kinds of surface relief structures or holographic structures are discussed, the term embossing is used. In the semiconductor, or the electronics industry, the term imprinting is more often used. Despite the differences in terminology, the basic process in both of the technologies is the same.

In recent years, the use of NIL has also been studied for optics, or more appropriately, for optoelectronics. If diffractive optics were replicated on active components on a wafer level, the costs for DOEs would be further reduced. The most promising class of active components include VCSELs, LEDs and image sensors. By replicating micro lenses or other diffractive optics elements directly on them, monolithic systems are produced that do not need any further optical alignment and assembly [14].

A key benefit of nanoimprint lithography is its sheer simplicity. There is no need for complex optics or high-energy radiation sources. There is also no need for finely

tailored photo resists designed for both resolution and sensitivity at a given wavelength. The simplified requirements of the technology also lead to its low cost, which is another key benefit. Since large areas can be imprinted in one step, this is also a high-throughput technique [15].

Rossi *et al.* [14] have developed a wafer level replication method that is based on NIL and which also enables the double-sided replication of a substrate. The process is commercialised using the brand name REEMO. The REEMO process governs all the steps from optical design to production [14]. However, REEMO is not used on LED wafers, or on other active components at present, but is more a fabrication method of diffractive optics on fused silica wafers, as shown in figure 7.1, for example.

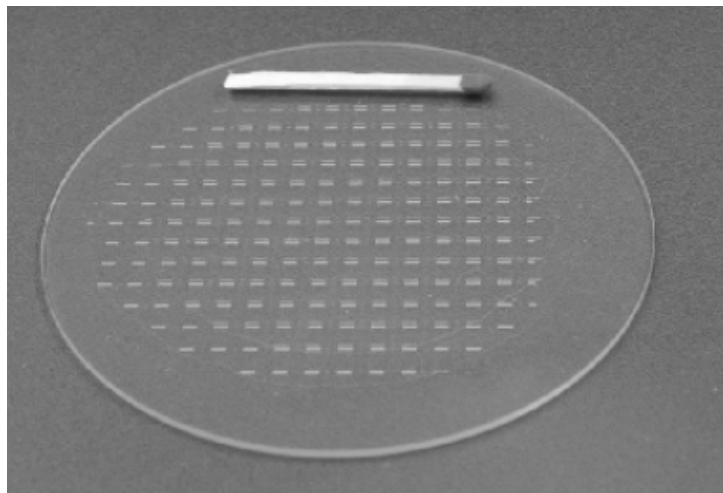


Figure 7.1. A 4" wafer containing replicated diffractive optics elements [14].

7.1 Methods for improving LEDs' external quantum efficiency

Ordinary LEDs out-couple only a fraction of the generated light, meaning the external quantum efficiency of a LED is far less than 10%. For example, for a GaAs LED, whose RI is 3.6, the critical angle of total internal reflection is 16° , resulting in the extraction of only 2% of the generated light per out-coupling surface in conventional LED structures. Several research groups have investigated this matter, and developed a variety of solutions for improving the efficiency. Most of the solutions are based on modulating the surface texture of the die. For a significant improvement in external

efficiency, it is necessary to change the angle under which the internally generated light sees the semiconductor surface [16].

For light incidence below the critical angle of total internal reflection, the transmission through a textured surface is reduced, compared to a flat surface. However, due to surface texturing, transmission becomes possible for incidence angles above the critical angle. As a result, internal scattering during internal reflection at the textured surface, is not necessary for an efficient extraction of the light generated inside the LED structure [16].

A research group led by Reiner Windisch has improved the quantum efficiency of a LED, reaching the level of 43% for unencapsulated LEDs and 54% after encapsulation. Furthermore, at low temperatures, the efficiency of unencapsulated devices increased to 68%. The LED is depicted in figure 7.2, showing the binary structure that was fabricated by dry etching it onto the surface [16].

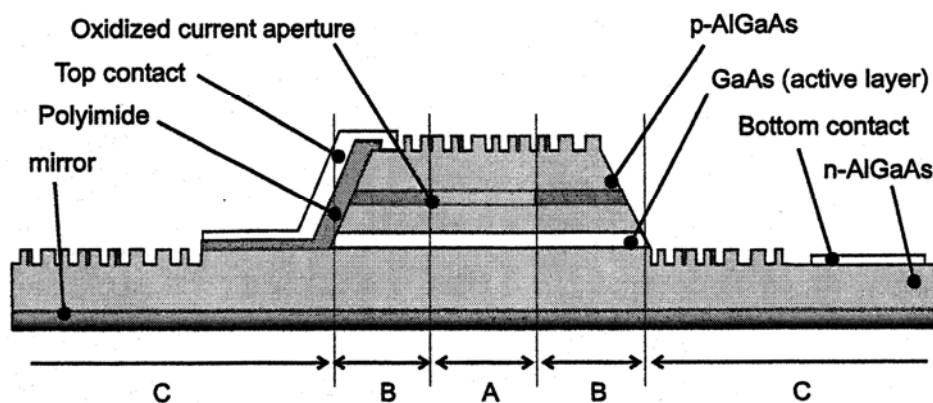


Figure 7.2. Surface textured LED. The pillars are ~200 nm high and are positioned at ~430 nm from each other [16].

Similar structures to improve the quantum efficiency have been used by N. Linder [17] and C. Rooman [18]. Erchak *et al.* [19] on the other hand, have used photonic crystals to improve the coupling. Enhanced coupling to vertical radiation is obtained using a two-dimensional photonic crystal that lies entirely inside the upper cladding layer of an asymmetric quantum well structure. A six-fold enhancement in light extraction in the vertical direction is obtained without the photonic crystal penetrating the active material [19]. The structure is shown in figure 7.3.

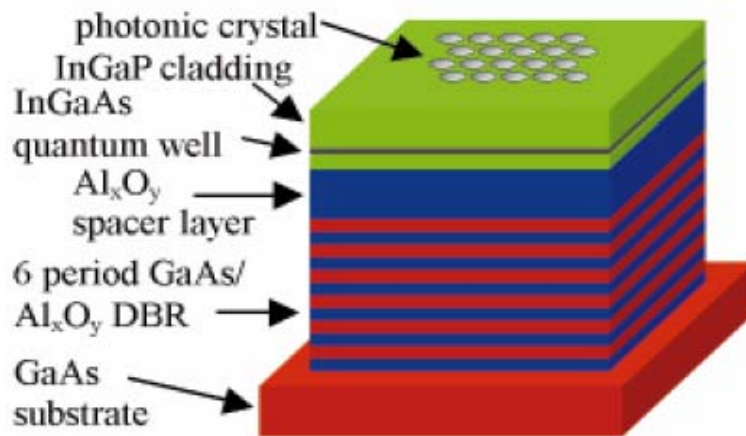


Figure 7.3. A LED with photonic crystals. The holes are 50 nm in radius and 340 nm apart from each other [19].

7.2 An imprinting approach

All of the improvement ways presented above are based on the texturing of the semiconductor material itself, thus requiring multiple process steps to achieve the desired result. Modines however, is developing NIL-based technology, where the nanostructure would be imprinted on the LEDs rather than etched onto it. There are UV curable resins on the market that have refractive indices over 2. These materials are used only as very thin layers that do not exceed 200 nm or so. Of course, it is not possible to arrive at such increase in external quantum efficiency other than by texturing the semiconductor material, because of the existing difference in the RI values, but respectively, the fabrication costs are substantially reduced, due to the simple process.

Modines is collaborating with the Technical Research Centre of Finland, VTT, to identify the process concept for this technology. SÜSS MicroTec with the cooperation of VTT, is developing a manufacturing machine called a SÜSS NPS300 NanoPatterning Stepper that is designed for UV-NIL and step hot embossing applications. The NPS300 achieves a sub-20 nm resolution, which makes it perfectly feasible to use NIL on LEDs. The machine is capable of handling 8" wafers and pressing tools up to 40 x 40 mm in size for NIL applications, and 100 x 100 mm for step hot embossing applications. The pressing force varies from 5 N to 4 kN [20].

7.2.1 Demonstration of the process

Figures 7.4 – 7.6 show the NIL process and results. First, substrate preparation is required, prior to the spin coating of the appropriate resist. The wafer is washed, and placed in an oven at a temperature of 200 °C for 30 minutes to dry. Next, the resist is spin-coated on the wafer, which is then placed on a hotplate for 2 minutes at 120 °C. The resist thickness should be around 300 nm. The resist used in this process was a colourless thermoplastic polymer that has a T_g value of 60 °C. Imprinting is then performed by placing the tool containing the microstructure in contact with the wafer. It is performed at 125 – 150 °C for 2 – 5 minutes, and a pressure of 5000 kPa is applied [21]. This is illustrated in figure 7.4. If it is assumed that the area being imprinted was the same as that used in step hot embossing, that is, 0.8 mm², the force required to achieve 5000 kPa pressure is only 4 N.

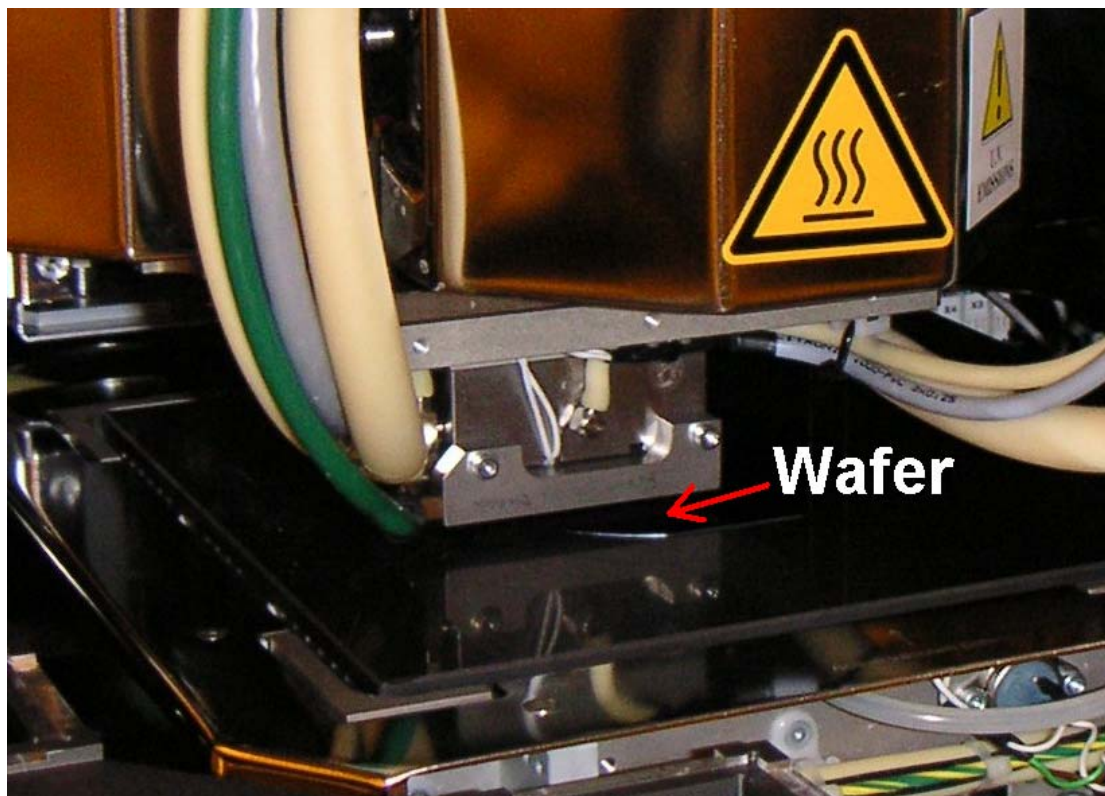


Figure 7.4. A wafer being imprinted. Courtesy Tomi Haatainen.

The tool is then detached at a release temperature of 50 – 60 °C [21]. Figure 7.5 shows the wafer, on which imprinting has been performed, and in figure 7.6 the structures are presented in more detail.

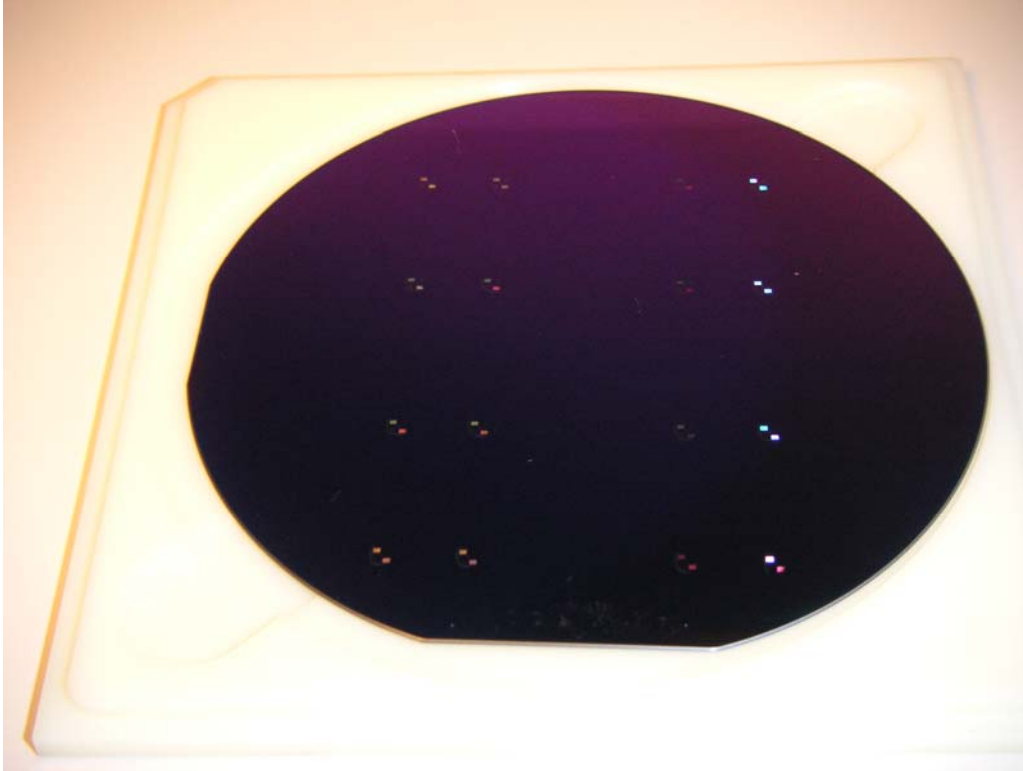


Figure 7.5. Imprinted wafer showing the microstructures on the resist. Courtesy Tomi Haatainen.

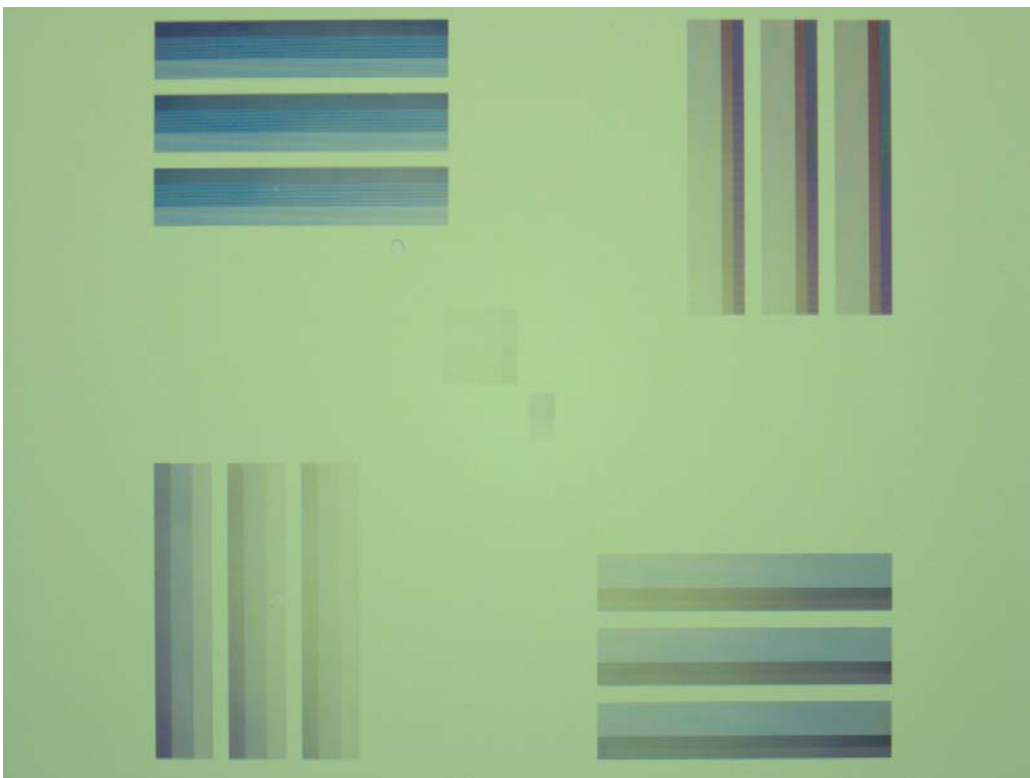


Figure 7.6. A microscope image of the imprinted structures on a wafer. Courtesy Tomi Haatainen.

The smallest linewidths in figure 7.6 are 1 μm . However, this imprinting machine reaches sub- 20 nm resolution, so successful fabrication of the imprinting tool is the key factor for successful NIL on LED wafers, for example.

8 Applications

In this chapter, some applications that could take advantage of the technologies presented in this thesis are briefly discussed. The most valuable things that are gained by using diffractive optics elements are the diminished size of a product, durability, flexible design, decrease in power consumption and the capacity for replication, which lowers manufacturing costs. The opportunities for applying DOEs are endless.

8.1 Advertisements

A variety of information and advertisement displays will probably be the first applications where DOEs are applied. At present, large amounts of LEDs are used for illumination in large advertisement displays.

Information and Ad-Displays



Figure 8.1. Different fields of advertisement displays are big business for LED-integrated diffractive optics elements [13].

8.2 Consumers

Figure 8.2 illustrates some applications aimed at consumer markets.

Consumer products



Figure 8.2. Applications directed at consumer electronics [13].

All of the above applications use LEDs for illumination. For example, keypads for mobile phones are illuminated with 6 to 12 LEDs. Using DOEs, this amount can be reduced to just one, which significantly reduces power consumption of the mobile phone. Additionally, the uniformity of the light on the keypad surface can be made better. Using the asymmetric placement of microstructures, large, enhanced backlight panels can be applied to LCD TVs.

8.3 Automotive

The automotive industry is one of the most attractive markets for DOEs because there are several possible targets for their use. Figure 8.3 shows some examples.

Automotive industry



Figure 8.3. Backlight systems in vehicles [13].

Flexible design enables DOEs to be applied in the automotive industry. Using them in rear lights, for example, the durability of the light is notably increased.

8.4 Traffic

Traffic



Figure 8.4. Traffic lighting is one important application fields for DOEs [13].

Old traffic lights are becoming widely replaced by LED technology. However, these lights use multiple LEDs to achieve the required efficiency. Using one high-bright LED combined with a large DO lens, the same light efficiency can be obtained with much lower power consumption and a smaller depth dimension. This is shown in figure 8.5. The lens gathers the light onto its whole surface and aims it forward. This assembly can also be used in backlight systems in vehicles.

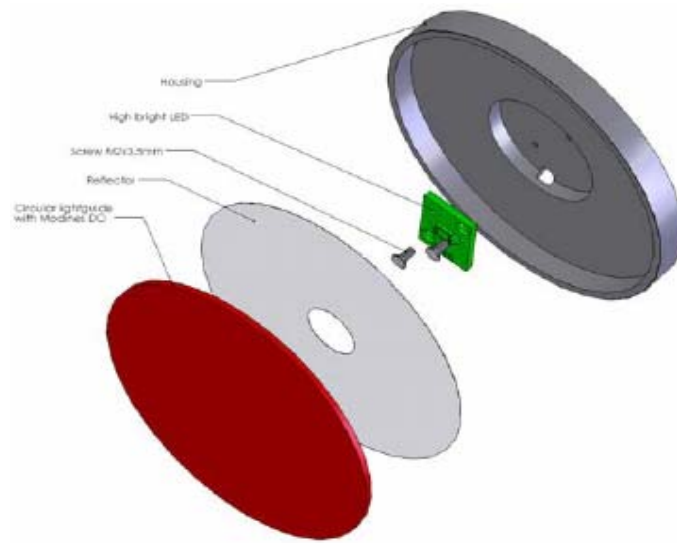


Figure 8.5. A large collimation lens with diameter of 11 cm. The parts from right to left are: housing, high bright LED, reflector and light guide with diffractive optics [13].

9 Conclusions and outlooks

The field of this thesis is very applicable – it extends from the replication of diffractive optics structures used in illumination and light collimation to an area of industrialization. The demand for these applications is huge, and solutions for them are given.

To give a good overview of this thesis, table 9.1 sums up the most important aspects that were discovered during this work.

Table 9.1. Technologies and their properties used in this work.

	Functionality of the technology	Industrialization	Cost-benefit
Diffractive optics lens replication	Really good	Feasible	Really good
Step hot embossing	Excellent	Feasible	Excellent
Nanoimprint lithography	Highly promising	Needs more research	Good

It has been shown that the replication and embossing methods and technologies are well suited to industrial manufacturing, because all the experiments and gained results were successfully conducted using a mass production bonder machine. Although nanoimprint lithography is still at the developing stage, it has been demonstrated that the procedure itself already works.

The issue of cost-benefit is probably the main concern for a manufacturer to industrialize a given technology. It is clear that the fabrication of a master tool can be expensive. But diffractive optics structures can be replicated many times with good fidelity, and thus the amount of products that can be produced will rapidly cover the expenses of the master tool.

The possibility of replicating illuminative microstructures on a thin film enables the film to be used in variety of applications, ranging from large backlight panels used in LCD televisions to smaller applications like focused illumination of keypads in handheld devices. The key factor to the success of the presented technology is the

successful fabrication of the structure on a replication tool, because with a good tool, the quality of replication will be also good. It is evident that with straightforward and logical experiments, the best replication parameters can be found, thus improving quality already.

A second important issue that was demonstrated in this work was the successful integration of diffractive optics lenses straight onto LEDs. This is an important result, that will be of great interest to a wide range of LED manufacturers, for example – in fact, it already has. Materials used in the process have a vital role in the performance and light out coupling of LEDs, and this is a field that is constantly developing. Thus, this issue must be continuously observed.

Naturally, there are issues that have to be solved prior to mass production and usage of these presented applications and technologies. For example, the question about the protecting of the lenses is open, as well as the materials' behaviour in large surface area replication. Environmental and reliability tests would be the next subjects of investigations, which are not taken into account in this thesis.

The use of diffractive optics will most certainly increase in the future. Because energy consumption increases in coming decades, and the used resources are draining, solutions must be found to reduce the consumption. One way to do this is by utilising diffractive optics combined with LEDs. For example, light pollution is an important issue that must be solved. The amount of energy that is lost in dispersed lighting is enormous. By focusing light only where it is needed, huge savings in energy can be obtained.

All the contents of this thesis has the same goal – improved illumination and quality of life. The only way to succeed in this is with interdisciplinary collaboration with different fields of researchers and manufacturers.

10 References

- 1 CIR reports: HB-LED applications- what customers want: A five-year forecast of OEM buyer requirements. January 2004.
- 2 <http://www.lightemittingdiodes.org> Chapter 12, visible spectrum LEDs. Accessed 18.8.2006.
- 3 Sami Franssila. Written notification, 13.7.2006.
- 4 Michael T. Gale, Markus Rossi, Hartmund Rudmann, Jyrki Saarinen and Marc Schnieper. Applications of replicated diffractive optical elements in consumer products. Presented at MOC'04 conference, Jena, 2004.
- 5 Frederik Nikolajeff. Diffractive optical elements: fabrication, replication and applications, and optical properties of a visual field test. A dissertation at Chalmers University of technology, department of microwave technology. Goteborg, 1997. Technical report No. 300. ISBN 91-7197-448-2.
- 6 Konstantins Jefimovs. Fabrication of surface relief diffractive optical elements and their applications. A dissertation at University of Joensuu, department of physics. Dissertations 40. ISBN 952-458-382-8.
- 7 Jari Lautanen. Fabrication of surface relief gratings and their applications in diffractive optics. A dissertation at University of Joensuu, department of physics. Väisälä laboratory. Dissertations 23. ISBN 951-708-947-3.
- 8 Wikipedia, the free encyclopaedia. Headword roll-to-roll.
- 9 An OSRAM power TOPLED datasheet. http://catalog.osram-os.com/media/en/Graphics/00016835_0.pdf accessed 19.7.2006.

- 10 An OSRAM power TOPLED datasheet. http://catalog.osram-os.com/media/en/Graphics/00016814_0.pdf accessed 28.7.2006.
- 11 Ilkka Mellin. Written notification, 19.6.2006.
- 12 David R. Lide, Ph.D. CRC Handbook of chemistry and physics. ISBN 0-8493-0483-0.
- 13 Oy Modines Ltd. technical presentation.
- 14 Markus Rossi, Hartmund Rudmann, Brigitte Marty, and Andreas Machiossek. Wafer scale micro-optics replication technology. Presented at SPIE conference on lithographic and micro machining techniques for optical component fabrication, 2003, San Diego.
- 15 Wikipedia, the free encyclopaedia. Headword nanoimprint lithography.
- 16 Reiner Windisch, Stefan Meinschmidt, Gathleen Rooman, Lars Zimmermann, Barun Dutta, Maarten Kuijk, Peter Kiesel, Gottfried H. Döhler, Gustaaf Borghs and Paul Heremans. Light extraction mechanisms in surface-textured light-emitting diodes. Proceedings of SPIE Vol. 4278 (2001).
- 17 N. Linder, S. Kugler, P. Stauss, K.P. Streubel, R. Wirth, H. Zull. High-brightness AlGaInP light-emitting diodes using surface texturing. Proceedings of SPIE Vol. 4278 (2001).
- 18 C. Rooman, R. Windisch, M. D'Hondt, P. Modak, I. Moerman, P. Mijlemans, B. Dutta, G. Borghs, R. Vounckx, M. Kuijk, P. Heremans. High-efficiency 650 nm thin-film light emitting diodes. Proceedings of SPIE Vol. 4278 (2001).
- 19 Alexei A. Erchak, Daniel J. Ripin, Shanhui Fan, Peter Rakich, John D. Joannopoulos, Erich P. Ippen, Gale S. Petrich and Leslie A. Kolodziejski. Enhanced coupling to vertical radiation using a two-dimensional photonic

crystal in a semiconductor light-emitting diode. Applied physics letters, volume 78, number 5.

- 20 SÜSS MicroTec press release. Apr-04-2005.
http://www.suss.com/main.php?rad_id=824 accessed 24.7.2006.
- 21 Micro resist technology. Datasheet of mr-I 7000 Thermoplastic Polymer for NanoimprintLithography.
<http://www.nanotech.ucsb.edu/NanotechNew/processing/Lithography/Materials/mr-I-7000.pdf> accessed 23.8.2006.
- 22 Fredrik Nikolajeff. Written notification, 17.8.2006.